Wood identification and anatomical investigation using X-ray CT and image analysis

2023

Hairi Cipta

Table of Contents

List of Abbreviations

ASM	: Angular second moment
CT	: Computed tomography
GLCM	: Gray level co-occurrence matrix
IAWA	: International Association of Wood Anatomists
PIV	: Particle image velocimetry
SEM	: Scanning electron microscopy
SPring-8	: Super Photon ring-8 GeV
SRX-ray μCT	: Synchrotron X-ray microtomography
SVM	: Support vector machine
X-ray CT	: X-ray computed tomography
2D-FFT	: Two-dimensional fast Fourier transform

Chapter 1 General Introduction

1.1.Overview

Over thousands of years, wood has played a significant role in human civilization. Since then, people have tried to understand what kind of wood is suitable fit to their needs. Human used wood for transportation, weaponry, building structure, statues, and a variety of other purposes. Nowadays, as organic material, many wooden objects disappeared because of chemistry recycling (Nilsson and Rowell, 2012). Some of them survive and become sources of information to study past civilization. Study about wooden artefact can enrich our knowledge about the development woodworking technology in the past, flora distribution, and even important climate event based on tree-ring pattern. To study about wood utilization in the past, information about wood species is important. There are numerous methods to identify wood species. One frequent technique is to examine the macroscopic and microscopic characteristics of wood anatomy (Hoadley, 1990; Wheeler and Baas, 1998).

The application of X-ray computed tomography (X-ray CT) in wood science was studied in this thesis. The identification of wood species to make kris sheath was conducted using high resolution synchrotron X-ray microtomography (SRX-ray μCT) (Chapter 2). By employing image analysis, development of wood classification model by analyzing CT images was conducted for 21 wood species that frequently used to make wooden statue and building in Japan (Chapter 3).

Instead using conventional microscopy technique, X-ray CT technique was also used to observe wood anatomical features of wood with interlocked grain, *C. camphora* (Chapter 4).

1.2.Wood anatomy

Wood can be referred as secondary xylem produced by coniferous gymnosperm and by dicotyledonous angiosperm (Donaldson et al., 2017). Anatomical structure of wood contains important information that can be useful to identify taxa (Abe, 2016), predict wood properties (Leonardon et al., 2010), examine past climate conditions (Worbes, 2011), find tree breed with superior quality, tackle illegal logging (Liu et al., 2022), etc. Wood anatomy combined with chemical composition and ultrastructure will determine the properties of wood (Donaldson, 2008; Donaldson et al., 2017).

In a gymnosperm and angiosperm trees, wood has two main functions, to transport water from the roots to the leaves and to support branch and crown of trees. Main differences of this two groups are the complexity of cell types that composed the secondary xylem. In gymnosperm, the secondary xylem composed by tracheid and parenchyma. However, more than 90% of the total number of cells is tracheid (Rathgeber et al., 2016). Mechanical and water conduction function is performed by tracheid cells. While, parenchyma will take care of storage and radial transport. In angiosperm, various types of cell exist with different function which are fiber cells, parenchyma cells, and vessel elements. Mechanical support function

by provided by fibers, water conduction function provided by vessel, and parenchyma cells as storage.

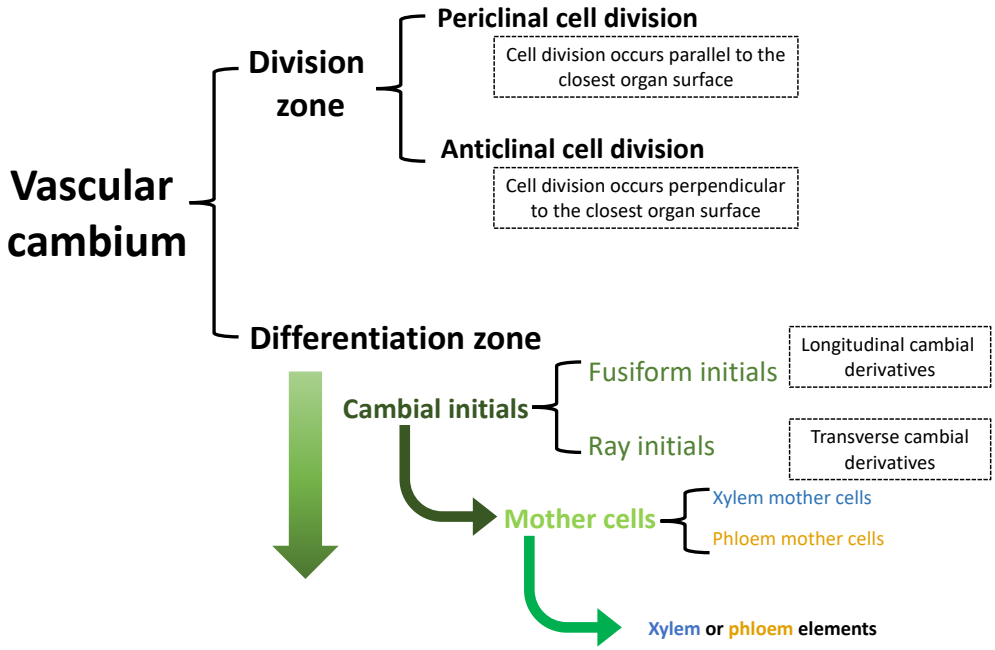

Figure 1.1. Two zones of vascular cambium: division zone and differentiation zone. Figure was modified from Ramos and Regan (2018)

The wood or secondary xylem are formed by division vascular cambium (Figure 1.1) (Ramos and Regan, 2018). When cambium cells divide parallel to or perpendicular to the closest organ surface, the cambium cells will remain in the layer and advance outward. Division of cambium cell inward will form secondary xylem tissue and division of cambium cell outward will form secondary phloem tissue. After the division, xylem cells will enlarge and differentiate into mature functional wood cells. The arrangement of mature cells somehow shows species-

specificity that will be useful for wood identification. Knowledge and understanding on wood anatomy will be useful for wood identification.

1.3.Wood identification

Different taxa will have different pattern of variation of cells shapes and morphology of cell types diversity of cells spatial distribution, allow to recognize plant taxa by analyzing the wood tissues (Wheeler and Baas, 1998). To help identification of wood, key characteristics based on wood anatomical features has been introduced for hardwood (IAWA Committee, 1989) and softwood (IAWA Committee, 2004) by International Association of Wood Anatomists (IAWA).

Wood identification in practical will be useful in timber trade, preserving endangered species (He et al., 2020; Liu et al., 2022), understanding woodworking in the past (Fioravanti et al., 2017; Giachi et al., 2016; Heady et al., 2010), filtering pulp and paper material (Helmling et al., 2016), to use best protocol for wood processing (Wheeler and Baas, 1998) and others. Classical microtomy using histology wood preparation then observed using light microscopy is common technique to obtain important anatomical features (Carlquist, 2010). Recent advance is the use of machine learning as alternative tool to empower wood identification process (Liu et al., 2022).

For wooden historical building or artefact in cultural heritage objects, we will obtain information about woodworking technology, ancient trade routes and environmental condition in the past (Fioravanti et al., 2017; Giachi et al., 2016). The challenge in wood identification of important object is to obtain enough sample

for microscopic observation (Heady et al., 2010). In some cases, it is prohibited to take sample from an important cultural object (Mizuno et al., 2010). If sampling is permitted, it may only be for a minimal amount of sample. To solve this problem, X-ray computed tomography (X-ray CT) is an alternative method to visualize the 3D structure of wood. X-ray CT technique can be used to observe internal structure of sample. Different resolution of X-ray CT source will be discussed in this thesis.

1.4.Interlocked grain phenomenon on *Cinnamomum camphora*

As mentioned earlier in 1.2 that history of tree growth strategy will be recorded in secondary xylem. The variation of wood properties in radial direction can be proxy to evaluate tree development and growth strategies to adapt and compete in certain environment. Wood grain patterns along tree radius is also seen as a tree growth strategy. Wood grain represents orientation of longitudinal elements in secondary xylem that is not always parallel to tree axis. Interlocked grain is one of phenomena when wood grain deviate from direction of tree axis that characterized by alternating left-hand spiral and right-hand spiral that take years before changing to the reverse direction (Harris, 1989; Krawczyszyn and Romberger, 1980; Kubler, 1991). For a living tree, one of functions of interlocked grain for living plant to improve strength of the wood (Hernandez and Almeida, 2003; Kojs et al., 2004). However, for woodworking, woods with interlocked grain is responsible for various problems (Leonardon et al., 2010).

According to earlier studies (Hernandez and Almeida, 2003; Kojs et al., 2004), interlocked grain phenomenon is common in a variety of tropical tree species,

including *Acacia mangium* (Ogata et al., 2003), *Hopea odorata* (Ogata and Fujita, 2005), *Amburana cearensis* A.C. Smith, *Lonchocarpus sericeus* (Poir.) DC. (Kojs et al., 2004), *Aspidosperma macrocarpon* Mart., and *Clarisia racemosa* Ruiz and Pav (Hernandez and Almeida, 2003).

Some methods have been introduced to investigate inclination in wood grain, such as splitting method, serial sectioning of tangential plane, confocal microscope, the inclined soft X-ray method (Krawczyszyn and Romberger, 1980; Martley, 1920; Ogata et al., 2003; Ogata and Fujita, 2005). In chapter 4, investigation of interlocked grain of *C. camphora* is discussed. X-ray CT was used to visualize 3D structure of *C. camphora* wood. Image analysis techniques were used to examine the interlocked grain.

1.5.X-ray computed tomography

X-ray computed tomography (CT) is a technique to observe three-dimensional and internal structure of an object without cutting it. X-ray CT can also be considered as a further development of two-dimensional (2D) radiograph technique. X-ray beam can be transmitted through an object. Then the transmitted radiation is recorded using film or currently collected as digital image. The series of 2D radiographs of the object seen from many different direction are reconstructed using an algorithm to create digital form of cross-section slices of the object (Withers et al., 2021). One major advantage of using X-ray CT for investigating cultural objects is that it is a non-destructive method. This means that the objects being scanned do

not need to be damaged in any way, allowing them to be studied and preserved for future generations.

In the beginning, X-ray CT was used for medical field (Landis and Keane, 2010). The first successful application of X-ray CT was in 1960s by Geoffrey Hounsfield and Allan Cormack (Casali, 2006). For their invention and contribution, they got Nobel Prize in Physiology and Medicine in 1979. Nowadays, X-ray CT technique is not only used for medical imaging. It is widely available in the market and used for many purposes, including in archaeology, material science, and wood science.

Table 1.1 Properties of X-ray CT from different X-ray sources (Lehmann and Mannes, 2012; Rankin et al., 2021)

	Standard X-ray CT with X-ray tube	Synchrotron source
Advantage	Flexibility to observe any size of object	High spatial resolution and high contrast
Disadvantage	Low energy will cause long exposure time. High energy will cause low contrast	Limited to very tiny sample size.
Area of application	Structure analysis in macroscopic to microscopic scale	Structure analysis in microscopic scale

CT uses a various of X-ray sources, including synchrotron and X-ray tubes (Landis and Keane, 2010; Stock, 2008; Withers et al., 2021). Table 1.1 shows differences of two different X-ray CT sources. In the beginning of X-ray CT application, X-ray tube can produce fan beam (Landis and Keane, 2010). The scanning time can be faster in further development by invention of cone beam that

can be produced by X-ray tube. Development of synchrotron radiation as X-ray source has also great contribution. Synchrotron beam is produced by electron accelerators shaped like a large ring (Casali, 2006). One of the advantage of using synchrotron beam is the high flux that make shorter exposure time is possible (Brodersen, 2013; Chappard et al., 2006) and able to resolve very subtle variation in absorptivity of the object (Landis and Keane, 2010). Also, we are able to obtain spatial resolution up to micrometer level by using synchrotron X-ray. Synchrotron X-ray CT (SRX-ray μCT) uses parallel to scan object monochromatic beam. In the present thesis, term SRX-ray μCT will be used to refer the technique that used synchrotron as source of X-ray beam. In Chapter 2, use of SRX-ray μCT to identify wooden sheath of kris (Indonesian dagger) will be introduced. The CT images acquisition process was conducted at SPring-8 (Super Photon ring-8 GeV) facility in Japan, one of 3rd generation synchrotron facilities.

An image is combination of many pixel which every wood species that has different anatomical features might have different pixel intensity (Hwang and Sugiyama, 2021). It is also applying for X-ray CT images of wood. Therefore, image analysis can be used as an approach to conduct wood identification. In Chapter 3, image analysis will be discussed to classify 21 Japanese wood species that often used to make culturally important objects in Japan. In Chapter 4, particle image velocimetry (PIV) and two-dimensional fast Fourier transform analysis were introduced to examine phenomenon of interlocked grain on *C. camphora*.

1.6.Objective of the thesis

The purpose of this study is to demonstrate the use of X-ray CT to observe wood anatomical characteristics and identify wood taxa. Chapter 1 of this thesis is containing brief introduction about wood anatomy and X-ray CT.

In Chapter 2, SRX-ray μCT was used to identify the wood materials used for making cultural objects. The study aimed to identify wood materials that used as materials for Indonesian kris sheath by using SRX-ray μCT instrument at SPring-8 and find key characteristics for these wood species.

In Chapter 3, standard X-ray CT with lower spatial resolution was used to obtain 3D structure of 21 Japanese wood species that frequently used to make cultural important properties. The study was conducted by extracting density information and textural features of the wood species.

In Chapter 4, standard X-ray CT was used to examine phenomenon of grain deviation or known as interlocked grain on *Cinnamomum camphora*. Image analysis techniques, particle image velocimetry (PIV) and two-dimensional fast Fourier Transform (2D-FFT), were adopted to examine grain angle variation of *C. camphora.*

Chapter 2 Identification of the wood species in the wooden sheath of Indonesian kris by synchrotron X-ray microtomography

2.1. Introduction

Kris is the name of a traditional double-edged dagger from Indonesia. Some kris have straight blades, while others have curved blades. The kris blade has a distinctive pattern of welded layered metals on the surface (Salvemini et al., 2020). This dagger was initially used as a weapon, but it has evolved into a cultural object with distinctive historical and artistic worth. The modern form of the kris may have existed before the 14th century on the island of Java, Indonesia (Wijayatno and Sudrajat, 2011). In later centuries, the kris culture assimilated with the cultures of other nations in Southeast Asia.

Humans have used wood for thousands of years, including as weapons (Nilsson and Rowell, 2012). Wood is also used to manufacture parts of the kris. Although the blade of the kris is the most important component and several studies have been performed to investigate the blade (Nečemer et al., 2013; Salvemini et al., 2020), the wooden hilt and sheath are also integral parts (Figure 2.1a). When choosing the material for making a kris sheath to protect the kris blade, there are a few things to consider. There is a tendency that the type of wood used to make the kris sheath indicates the social status and philosophy of the owner. However, wood selection for the kris sheath has changed because of the scarcity of wood materials and other

factors. The valuable knowledge about the wood preference may disappear owing to this shift. Therefore, wood identification is crucial for preserving knowledge about the kris sheath. Nevertheless, identifying wood species of the kris sheath by scientific methods has not been widely performed.

Usually, wood identification is performed by observing anatomical characteristics of the wood. Therefore, a certain amount of sample needs to be removed from the object for observation. However, for cultural objects, sampling from the object must be carefully managed. Therefore, the minimum amount of the object needs to be removed, but the amount should be sufficient to understand the wood anatomical characteristics. For a relatively small sample, it is difficult to obtain an appropriate wood section. Scanning electron microscopy (SEM) is one option to observe a small sample (Heady et al., 2010). However, this procedure requires significant preparation that can damage the sample. Additionally, three orthogonal planes—the transverse, radial, and tangential planes—are typically used to observe the anatomical properties of wood. The SEM technique is not sufficiently adaptable to visualize the surfaces of these planes.

Combined low-resolution neutron and conventional X-ray computed tomography (CT) has been used to investigate kris sheath materials (Lehmann and Mannes, 2012). The advantages of this technique are the minimal effort for sample preparation and the possibility of reconstructing images in a volumetric way. In addition, sectioning in any direction is possible, which allows the important transverse, radial, and tangential planes of wood to be revealed. However, the resolution of this method is not sufficiently high to obtain the important

microscopic features for wood identification. Synchrotron X-ray microtomography (SRX-ray μCT) is an alternative method to obtain detailed microscopic features (Mizuno et al., 2010; Tazuru and Sugiyama, 2019) . Therefore, in this study, the wood species in the kris sheath were identified by using SRX-ray μCT. This technique is suitable for revealing the microscopic features of wood with minimum sample availability and without significant damage to the sample. Therefore, the sample can be used for other analyses. Additionally, segmentation based on the densities of the materials (Brodersen, 2013) can be performed to reveal the spatial distribution of the mineral inclusions in the xylem cells.

2.2. Materials and Methods

2.2.1. Wood samples and image acquisition

Seven Javanese kris sheaths were investigated, as shown in Figure 2.1b–h. In this study, each sample was assigned a number from 1–7 for identification purposes. The shapes of the sheaths are typical of the Javanese sheaths produced in the region near the Province of Central Java and Special Province of Yogyakarta in Indonesia. The first type is *gayaman*, which was carved like gayam fruit (*Inocarpus fagifer*) (Figure 2.1b, d, g, and h). The second type is *ladrang* or *branggah*, which was carved like the shape of a ship (Figure 2.1c, e, and f). Small wood fragments with a maximum diameter of 0.7 mm and 5 mm in length were extracted from the *warangka* part of each sample.

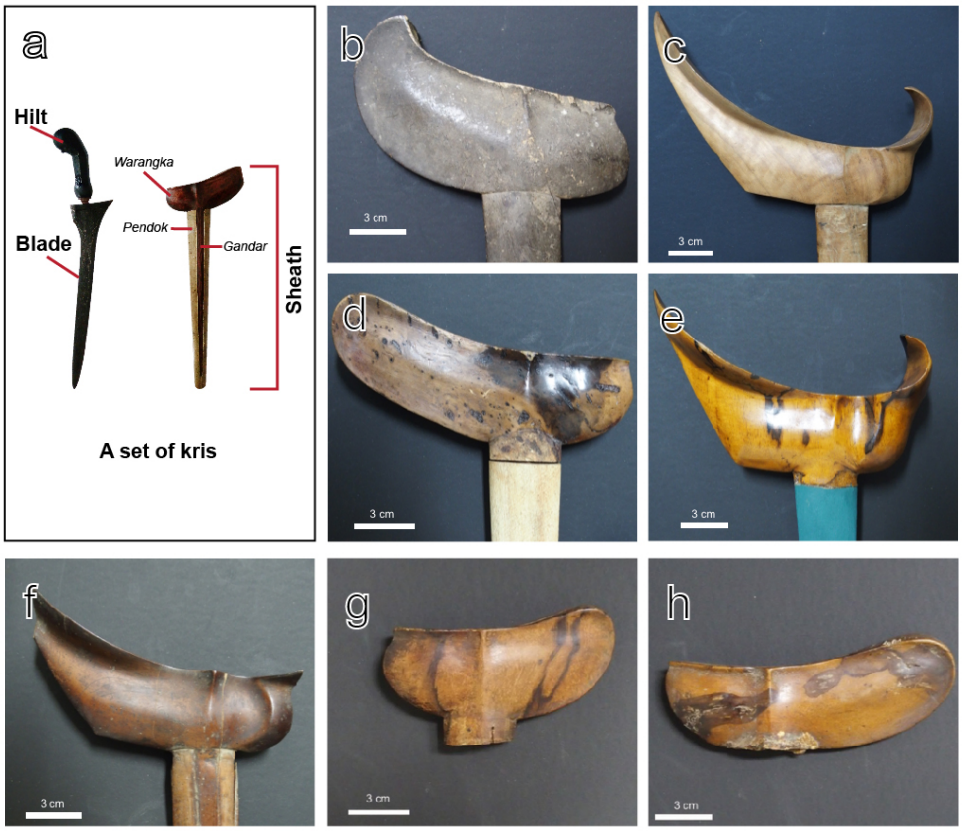

Figure 2.1. a Definition of the kris main parts. Photographs of the kris sheaths: **b** 1, **c** 2, **d** 3, **e** 4, **f** 5, **g** 6, and **h** 7. Numbers 1–7 were used as an identity for each kris sheath sample

CT data was obtained by performing SRX-ray μCT experiments at beamline 20XU of the SPring-8 facility in Harima, Hyogo Prefecture. Using a high-resolution camera, 1800 transmission images were recorded (2048 × 2048 pixels). Sheaths 1–5 were scanned with a resolution of 0.472 μm/pixel, and sheaths 6 and 7 were scanned with a resolution of 0.508 μm/pixel. The image data was reconstructed to convert the transmission images into cross-section image slices (2048 in total).

The images from the cross section were processed using the volume graphic software VGStudio MAX 2.2 (Volume Graphic GmbH, Heidelberg, Germany) to obtain three-dimensional (3D) images and a virtual section from different planes by virtually cutting the set of images. Most of the images were cut based on the three orthogonal planes of wood: the transverse, radial, and tangential planes. A single image slice (one pixel in thickness) only represents limited thickness of the real object. To optimize visualization of the CT images, pseudo-micrographs were prepared using the same software to obtain information from a thicker part by combining multiple slices in one image. Therefore, image visualization that approximates the depth information of an optical micrograph might be achievable.

2.2.2. Wood species identification

Wood species identification was started by examining the observable anatomical characteristics of the different planes by following the description of the International Association of Wood Anatomists (IAWA) (IAWA Committee, 1989). The online anatomical characteristic database provided by the online wood database InsideWood (InsideWood, 2004) was used to filter a number of species candidates. The wood identification key reference of Southeast Asia and the Western Pacific was also used (Ogata et al., 2008). Some publications were also referred to obtain additional information regarding wood selection to make the kris sheath. (Arifin, 2006; Frey, 2003; Harsrinuksmo, 2004; Moebirman, 1973).

Table 2.1. Identification results of likely species of wood used in the kris sheaths

Sheath No.	Number in **Fig. 2.1**	IAWA Code	Species prediction	Family
1	b	13, 22, 30, 47, 65, 80, 82, 85, 86, 97, 106, 115, 136, 142	*Dysoxylum* sp.	Meliaceae
2	c	13, 22, 30, 47, 65, 80, 82, 85, 86, 97, 106, 115,	*Dysoxylum* sp.	Meliaceae
3	d	13, 22, 30, 47, 58, 80, 81, 83, 97, 104, 115, 136, 142	*Tamarindus indica*	Fabaceae
4	e	13, 22, 30, 77, 97, 107, 111, 115, 136, 137, 138, 141	*Kleinhovia hospita*	Malvaceae
5	f	13, 30, 46, 65, 80, 86, 97, 115	*Dysoxylum* sp.	Meliaceae
6	g	13, 30, 47, 58, 80, 81, 89, 97, 104, 115, 136, 142	*Tamarindus indica*	Fabaceae
7	h	13, 22, 30, 48, 77, 97, 107, 111, 115, 136, 137, 138, 140, 141	*Kleinhovia hospita*	Malvaceae

2.3. Results

Some important anatomical features were extracted and visualized by the SRX-ray μCT technique combined with volume graphic software. The results are given in Table 1. Reconstructed images of the virtual sections in two dimensions of the samples obtained by processing the images from various planes using volume graphic software are shown in Figure 2.2. and 2.3. Finally, prediction of the wood species was performed based on the key characteristics of the anatomical features. Several microscopic anatomical features can be revealed using this technique, including the vessel characteristics (vessel grouping, perforation plate, and pit type), ray parenchyma characteristics (ray width, rays per millimeter, ray cellular composition, and ray cellular composition), axial parenchyma type, fiber type, and prismatic crystal location.

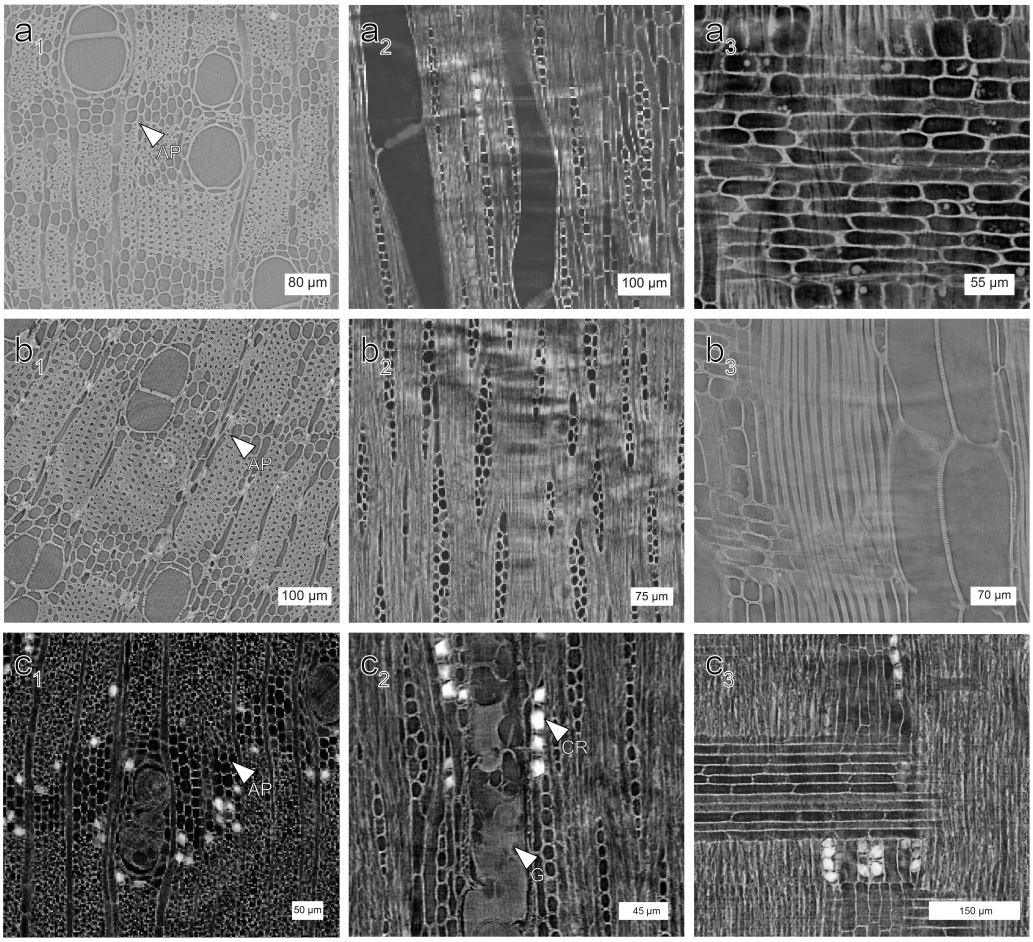

Figure 2.2. Virtual sections and 3D reconstruction of sheath (**a**$_1$–**a**$_3$) 1, (**b**$_1$–**b**$_3$) 2, and (**c**$_1$–**c**$_3$) 3. Transverse sections (**a**$_1$, **b**$_1$, **c**$_1$), tangential sections (**a**$_2$, **b**$_2$, **c**$_2$), and radial section (**a**$_3$, **b**$_3$, **c**$_3$). AP = axial parenchyma, CR = prismatic crystal, and G = gum

2.3.1. Sheaths 1, 2, and 5

The anatomical characteristics of kris sheaths 1, 2, and 5 were identified to be *Dysoxylum* spp. The vessels were solitary and in radial multiples of 2 (Figure 2.2a$_1$, 2.2b$_1$, and 2.3b$_1$). The perforation plate was simple. The intervessel pits were alternate. The vessel-ray pits were similar to the intervessel pits, and the rays were 1–2 cells in width (Figure 2.2a$_2$ and 2.2b$_2$). The number of rays per millimeter was

7–9, and the cellular composition of the rays was body ray cell procumbent with one row of upright and/or square marginal cells. The axial parenchyma types were winged-aliform narrow bands, and the bands were more than three cells wide (Figure 2.2a_1, 2.2b_1, and 2.3b_1). Septate fibers were observed in all of the samples, but they were more dominant in sheath 5 (Figure 2.3b_2). Prismatic crystals were absent for sheaths 2 and 5, but a few prismatic crystals were observed in sheath 1. The crystals were located in chambered axial parenchyma cells (Figure 2.2a_2).

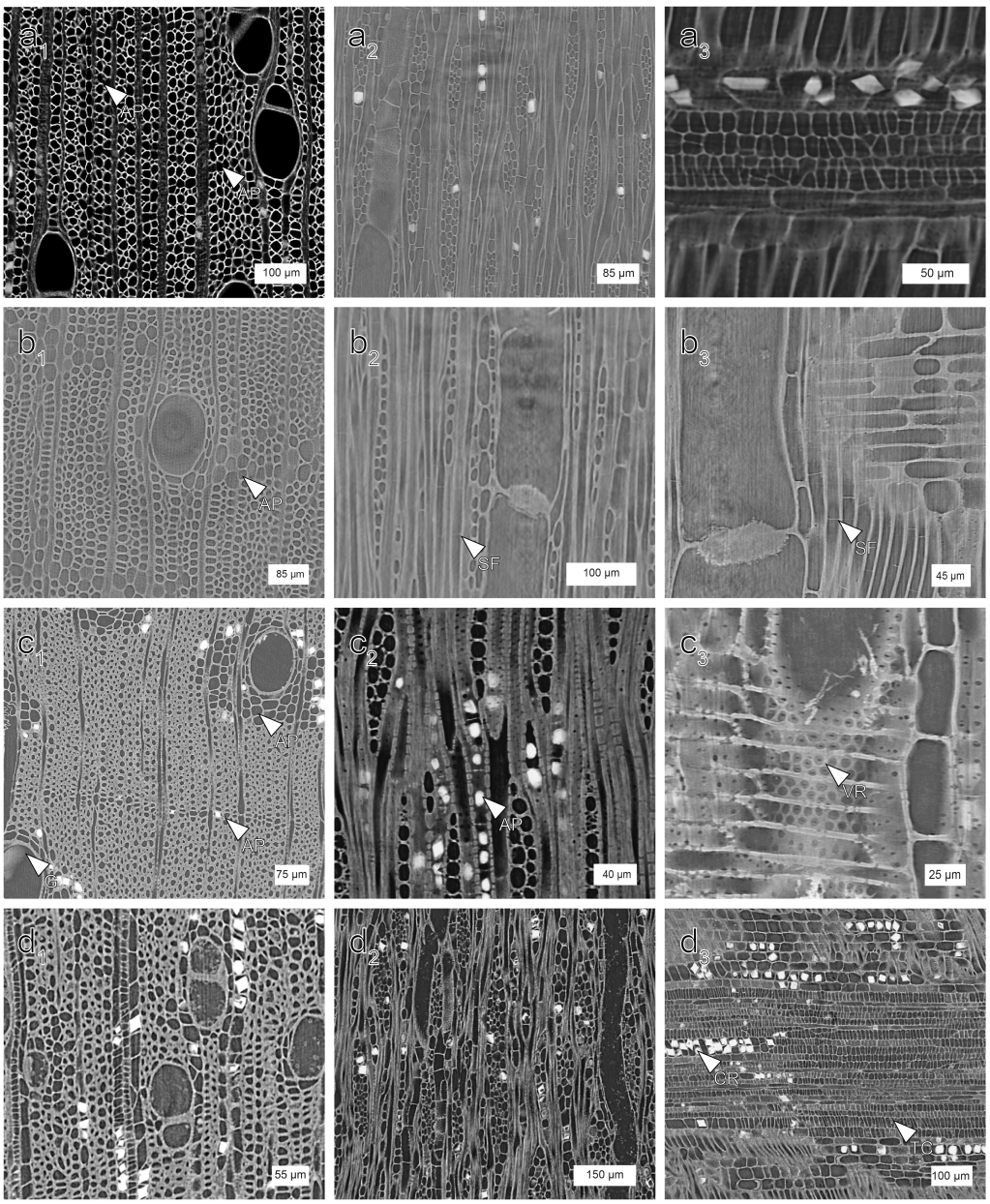

Figure 2.3. Virtual sections and 3D reconstruction of sheaths (**a**$_1$–**a**$_3$) 4, (**b**$_1$–**b**$_3$) 5, (**c**$_1$–**c**$_3$) 6, and (**d**$_1$–**d**$_3$) 7. Transverse sections (**a**$_1$, **b**$_1$, **c**$_1$, **d**$_1$), tangential sections (**a**$_2$, **b**$_2$, **c**$_2$, **d**$_2$), and radial sections (**a**$_3$, **b**$_3$, **c**$_3$, **d**$_3$). AP = axial parenchyma, SF = septate fiber, VR = vessel-ray pits, CR = prismatic crystal, G = gum, TC = tile cell

2.3.2. Sheaths 3 and 6

The anatomical characteristics of sheaths 3 and 6 belonged to *Tamarindus indica*. The pseudo sections of the samples are shown in Figure 2.2$c_{1–3}$ and 2.3$c_{1–3}$. The vessels were solitary with radial multiples of 2–3 (Figure 2.2c_1 and 2.3c_1). The perforation plate was simple. The intervessel pits were alternate. The vessel-ray pits had distinct borders (Figure 2.3c_3). Gum or other deposits were present in the vessels (Figure 2.2c_2 and 2.3c_1). The rays were 1–2 cells in width, and the type of ray cells was procumbent (Figure 2.2c_3). The number of rays per millimeter was 11–12. The axial parenchyma types were lozenge-aliform and confluent (Figure 2.2c_1 and 2.3c_1). In addition, axial parenchyma in marginal bands was present in sheath 6 (Figure 2.3c_1). The fiber was non-septate. There were abundant prismatic crystals (Figure 2.2c_1 and 2.3c_1), and the prismatic crystals were distributed in the chambered axial parenchyma cells (Figure 2.2c_2 and 2.3c_2).

2.3.3. Sheaths 4 and 7

It was predicted that the wood species used to make sheaths 4 and 7 was *Kleinhovia hospita*. The vessels were solitary and in radial multiples of 2–3 (Figure 2.3a_1 and 2.3d_1). The perforation plate was simple. The intervessel pits were alternate. The vessel-ray pits had distinct borders. The rays were 1–4 cells in width (Figure 2.3a_1 and 2.3d_1), and they were composed of body ray cell procumbent with 2–4 rows of upright and/or square marginal cells. The number of rays per millimeter was 8–9. Tile cells were found among other types of ray cells (Figure 2.3a_3 and 2.3d_3). The axial parenchyma type was diffuse-in-aggregate (Figure 2.3a_1).

Prismatic crystals were distributed in chambered (Figure 2.3d_3) and non-chambered (Figure 2.3a_3) upright and square ray cells (Figure 2.3a_3), as well as in non-chambered axial parenchyma.

2.3.4. Spatial distribution of the prismatic crystals

The presence of crystals is often used as a useful feature for identification purposes. In addition to visualizing the existence of crystals, the advantage of using X-ray CT is the ability to visualize their arrangement in 3D, which is not possible using conventional sectioning methods.

Abundant prismatic crystals were observed in the samples of sheaths 3, 4, 6, and 7. The samples belonged to two species: *T. indica* (sheaths 3 and 6) and *K. hospita* (sheaths 4 and 7). The patterns of the crystals for these two species were different. Generally, two types of distributions were observed: longitudinal alignment of the crystals inside the axial parenchyma cells for *T. indica* (Figure 2.4) and radial alignment of the crystals inside the ray cells for *K. hospita* (Figure 2.5). The distribution of crystals inside the axial parenchyma cells with aliform type is shown in Figure 2.4. In the aliform type, the axial parenchyma cells were distributed around the vessels. Many crystals were longitudinally aligned inside the axial parenchyma cells around the vessels (Figure 2.4). Meanwhile, the prismatic crystals were extensively distributed in the ray cells of *K. hospita*, as shown in Figure 2.5. The crystals were grouped in radial alignment with short or long series. The crystal groups did not occupy entire ray cells, but they were scattered among non-crystal ray cells.

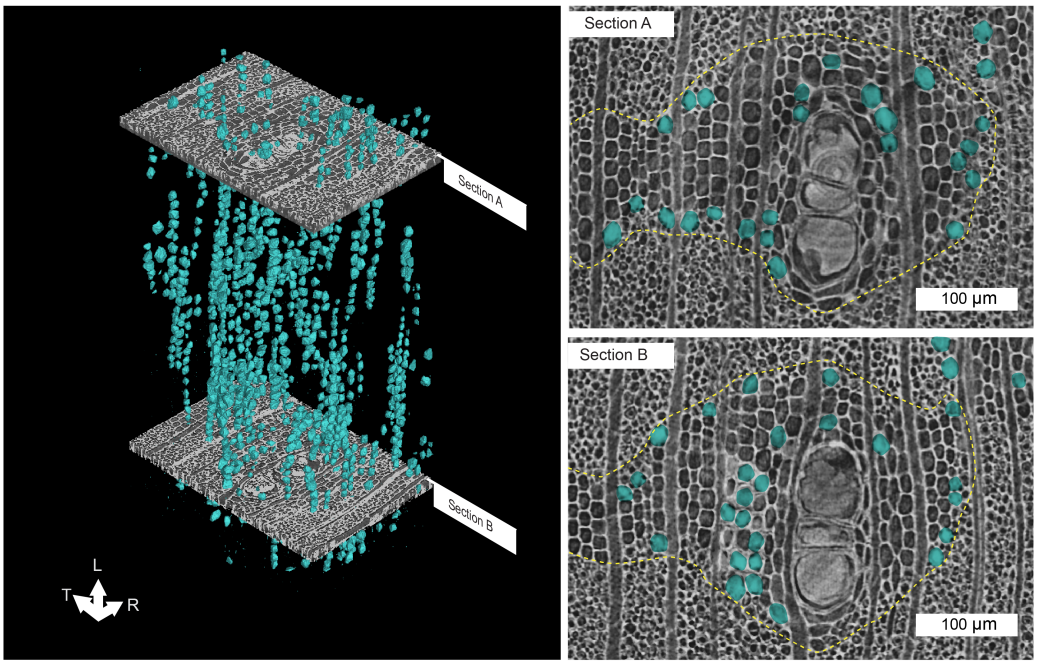

Figure 2.4. Spatial arrangement of the prismatic crystals surrounding the vessels in sheath 3. Left: 3D visualization of the wood by isolating the prismatic crystals (blue) and two consecutive transverse sections (sections A and B). Right: 2D views of sections A and B. The yellow dashed line is the boundary between the axial parenchyma and fiber cells.

2.4. Discussion

The wood species used for the wooden kris sheaths was identified based on the anatomical characteristics of samples of the sheaths by SRX-ray µCT. All of the samples were identified to be hardwood species (e.g., *Dysoxylum* spp., *T. indica,* and *K. hospita*) (Table 1). This is not surprising because only a few species of softwood belong to the families Araucariaceae, Pinaceae, and Podocarpaceae grown in Southeast Asia and the Pacific (Ogata et al., 2008). The wood species used for making sheaths 1, 2, and 5 contained septate fiber, which is commonly observed in the genus *Dysoxylum,* family Meliaceae. Several species in the Meliaceae family,

including some in the genera *Entandrophragma* and *Guarea,* have nearly identical anatomical features as *Dysoxylum*. However, based on their geographical origin, the samples are most likely from the genus *Dysoxylum*. Furthermore, *Dysoxylum acutangulum* has traditionally been utilized as kris sheath material (Haryoguritno, 2006). Septate fiber is a type of fiber with thin, unpitted, transverse wall (IAWA Committee, 1989; Ilvessalo-Pfäffli, 2010). Another characteristic of this genus is the appearance of banded axial parenchyma (Ogata et al., 2008). In sheaths 3 and 6, one of prominent characteristics of *T. indica* was the appearance of gum or other deposits in the vessels. In addition, crystals were present in the chambered axial parenchyma. The existence of tile cells for sheaths 4 and 7 is one of the key characteristics of *K. hospita*. Tile cells occur in only 1% of hardwoods (Wheeler and Baas, 1998), and they are an important characteristic in distinguishing the Malvales members. The type of tile cells of this species is *Durio* type. The tile cells in sheaths 4 and 7 had the same height as the procumbent cells (IAWA Committee, 1989).

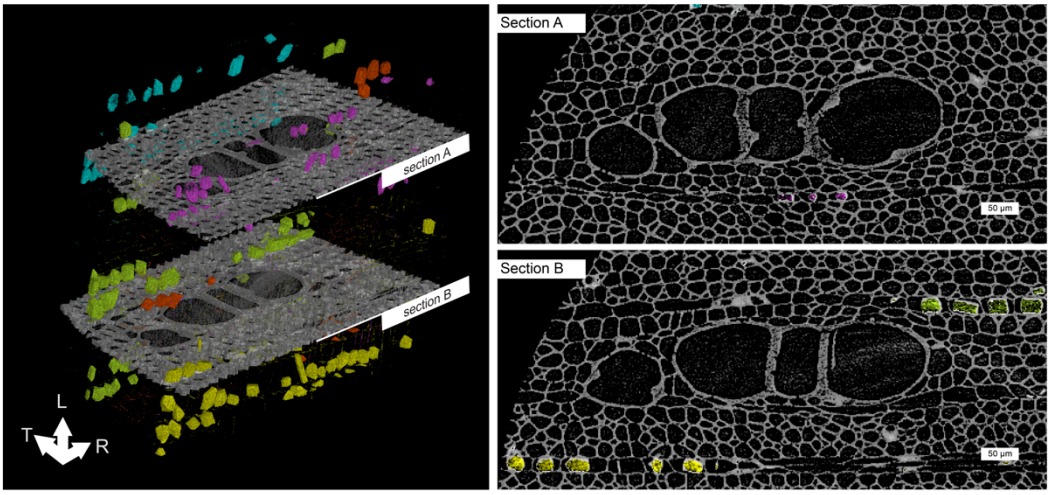

Figure 2.5. Spatial arrangement of the prismatic crystals surrounding the vessels in sheath 4. Left: 3D visualization of the wood by isolating the prismatic crystals (blue, green, red, purple, and yellow particles) and two consecutive transverse sections (sections A and B). The different colors of the particles show different tangential positions of the crystals. Right: 2D views of sections A and B.

In this study, part of the sample observed was approximately 1 mm in both diameter and length. With a small amount of sample, information about the wood porosity and growth-ring morphology that is important for wood identification may not be obtained (Heady et al., 2010). However, features such as the perforation plate, the morphology of pits, septate fibers, and tile cells could be obtained using SRX-ray µCT, which can be more time-efficient than using conventional sectioning methods. When using the sectioning method, some iterations are required to get appropriate sections to observe such features. However, these iterations will be difficult to apply due to limited sample availability. For SRX-ray µCT, infinite repeated sectioning is possible. Therefore, compared to traditional sectioning, SRX-ray µCT is better to have more successful wood identification with minimum sample size while keep the sample is still intact.

A kris sheath is typically made of selected materials. A high-quality kris sheath is usually made of fine, esthetic, rare, and expensive wood (Frey, 2003; Haryoguritno, 2006; Moebirman, 1973; van Duuren, 1998). Several wood species are often used for kris sheaths, such as *Santalum album, K. hospita*, *Dysoxylum acutangulum, Wrightia javanica, Melia azedarach, Murraya paniculata, Ficus septica, Dalbergia latifolia*, *Mesua ferrea, Tectona grandis, Cassia siamea, Pterocarpus indicus, T. indica*, and *Cassia laevigata* (Arifin, 2006; Frey, 2003; Harsrinuksmo, 2004; Haryoguritno, 2006; Moebirman, 1973). Sheaths 4 and 7 were *K. hospita* with dark-brown stains on their surfaces (Figure 2.1e and 2.1h). The appearance of a dark-brown stain was one of the considerations for selecting *K. hospita* (Haryoguritno, 2006). Sheaths 3 and 6, which were made of *T. indica*, also had dark-brown stains on their surfaces. Although *K. hospita* species can be identified through the appearance of a dark-brown stain, to avoid misidentification, observation of the wood anatomy is more accurate to distinguish the wood species. Meanwhile, *Dysoxylum acutangulum,* also known as *trembalo* (local name in Indonesia), is preferable because this species has a beautiful grain.

Generally, xylem tissue and the surrounding air provide sufficiently fine contrast when observed by SRX-ray μCT. Because mineral inclusions have higher density than xylem tissue, they can be identified in xylem cells (Vansteenkiste et al., 2007). The mineral inclusions with the prismatic crystal shape were reconstructed in volumetric space by performing simple segmentation. The crystal may have some functions, such as protection against insects, detoxification of toxic substances, tissue mechanical support, as well as light gathering and reflectance

(Carlquist, 2010; Franceschi and Horner, 1980; Franceschi and Nakata, 2005; Hudgins et al., 2003; IAWA Committee, 2016; Vansteenkiste et al., 2007). As previously mentioned, two different patterns of crystal distribution were observed. First, on *T. indica*, the crystals in longitudinal alignment in the axial parenchyma cells around the vessels as if they were pile foundation on a building structure. Second, radial short and long series of crystals were observed on *K. hospita* as if they were beams of load bearing wall on a building structure. Similar observation was conducted on bark structure and suggested that the presence of abundant prismatic crystals contributed as mechanical reinforcement to prevent compression fracture (Shibui and Sano, 2022). The spatial distribution of the crystals may influence the mechanical function to strengthen the structure of the vessel for water conduction in many species with axial parenchyma arrangements that encircle the vessel entirely (vasicentric, aliform, and others), mainly belonging to the family Fabaceae, including *T. indica.* The radial alignment of the crystals in *K. hospita* may be useful in strengthening the structure of the ray cells.

2.5. Summary

The wood species in the sheaths of Indonesian kris were identified. This study was the first attempt to identify the wood species in wooden kris sheaths based on microscopic observation of the anatomical features of the wood species. Small samples of seven kris sheaths were analyzed using SRX-ray μCT. Therefore, excessive wood sampling of the objects was avoided. Another advantage of this method is that the samples can be used for further analyses. This technique allowed

us to visualize the wood microstructure in the conventional orthogonal planes (transverse, radial, and tangential planes) in two dimensions, as well as to reconstruct the microstructure in three dimensions. For the seven wooden sheath samples investigated in the present study, sheaths 1, 2, and 5 were *Dysoxylum* sp., sheaths 3 and 6 were *T. indica*, and sheaths 4 and 7 were *K. hospita.* The SRX-ray μCT technique allowed us to reveal the spatial distributions of the prismatic crystals in *T. indica* and *K. hospita.* The distributions of the crystals were not random. The spatial arrangement of the crystals might have a mechanical function in certain cells.

Chapter 3 Wood classification based on density histogram and texture analysis with 2D GLCM

3.1.Introduction

In Japan, more than half of designated cultural properties made of wood. Wooden components of the objects will experience chemical and physical changes since they are organic materials (Nilsson and Rowell, 2012). Inspection of the properties is required to analyze their condition in order to determine how to manage the objects. X-ray computed tomography (CT) technique has been implemented widely to investigate important historical-cultural objects with minimum damage, including objects that made of wood. It is supported by availability of laboratory scale X-ray CT instrument at national museum (Araki, 2020). X-ray CT allow to visualize three-dimensional of an object that also provide information regarding inner part of the object (Lehmann and Mannes, 2012). The implementation of X-ray CT technique for cultural properties in Japan has resulted rich datasets of CT images of wooden cultural properties.

Wood species is a basic information for more advance study on cultural wooden artifact, for instance, to learn about wood selection and distribution of the species in the past period. Observation of wood anatomy has been widely used to identify a wood species. The conventional wood anatomical observation is usually performed by preparing a thin section then observed under a light microscope. The technique can reveal important key features that will be helpful for identification often observed from three orthogonal directions, i.e. transverse, radial, and

tangential direction (Ogata et al., 2008). Unfortunately, due to low resolution of CT images, it may be difficult to recognize wood anatomical features. Therefore, it is necessary to obtain other features to identify the wood species.

Performing machine learning is one of successful approach to identify species from CT images (Kobayashi et al., 2019, 2015) with help of textural analysis technique known as GLCM (gray level co-occurrence matrix) (Haralick et al., 1973). Meanwhile, extracting density information from CT images is also possible (Beaulieu and Dutilleul, 2019; Wang et al., 2019). Wood density and anatomical characteristics are related to each other (De Mil et al., 2018; Guilley et al., 2002; Zheng and Martínez-Cabrera, 2013). Therefore, in the present work, a research of wood classification using X-ray CT was carried out by extracting density data and textural traits from 21 Japanese wood species that are utilized to manufacture cultural properties in Japan.

3.2.Materials and Method

3.2.1. Wood samples

Wood samples of 21 species from the Xylarium of the FFPRI (Forestry and Forest Product Research Institute) were used in this study. The TWTw code address is assigned to each wood sample in the Xylarium. Selected wood samples based on raw material that frequently used to make sculpture and building in Japan (Kaneko et al., 2019, 2010; Kohara, 1972, 1964). Table 3.1 shows list of species name with TWTw registry number, dimension, and corresponding mean density.

Table 3.1. Wood specimens used in this study

Species	TWTw number	Size* (mm)	Mean density (g/cm^3)
Aesculus turbinata	870	143×48.5×242	0.507 ± 0.031
Betula maximowicziana	9304	150×49×199	0.668 ± 0.034
Betula platyphylla	9302	150×47×200	0.606 ± 0.057
Betula schmidtii	2569	160×47×245	0.683 ± 0.076
Buxus microphylla	2255	125×59×244	0.699 ± 0.027
Catalpa ovata	58	164×55×197	0.378 ± 0.017
Cerasus jamasakura	9333	146×41×200	0.555 ± 0.035
Cercidiphyllum japonicum	4339	156×44×246	0.517 ± 0.022
Chamaecyparis obtusa	9293	147×48×161	0.375 ± 0.035
Chamaecyparis pisifera	9294	148×48×133	0.32 ± 0.012
Cinnamomum camphora	909	153×45×245	0.477 ± 0.021
Cryptomeria japonica	9292	177×45×171	0.312 ± 0.014
Distylium racemosum	9332	147×48×199	0.755 ± 0.025
Machilus thunbergii	9331	148×49×199	0.542 ± 0.034
Magnolia obovata	28849	176×48×249	0.523 ± 0.045
Paulownia tomentosa	9346	178×48×232	0.324 ± 0.045
Pinus densiflora	844	149×50×244	0.46 ± 0.037
Pinus parviflora	851	139×58×178	0.42 ± 0.016
Pinus thunbergii	9288	135×57×217	0.601 ± 0.042
Torreya nucifera	9272	178×45×249	0.443 ± 0.029
Zelkova serrata	9326	148×48.5×197	0.541 ± 0.032

*length, width, height

3.2.2. X-ray CT and image acquisition

X-ray CT experiment was performed by using Y.CT Modular (YXLON International GmbH, Germany) with a small focused beam generated at 450 kV, 1.55 mA, installed at Tokyo National Museum. Flat detector Y.XRD1620 was used

to record the images. The volumetric gray-level data with voxel resolution 0.2615 mm was reconstructed using the instrument. For each CT scanning, three samples were observed simultaneously. A plastic bottle of water put at the center rotation of stage and the three samples are positioned in three radial directions, separated by 120 degree (Figure 3.1.). Longitudinal axis of wood was always placed along the rotation axis of the stage, and the width direction of the board in the radial direction of the stage. The CT datasets were processed using the volume graphic software VGStudio MAX 2.2 (Volume Graphic GmbH, Heidelberg, Germany.

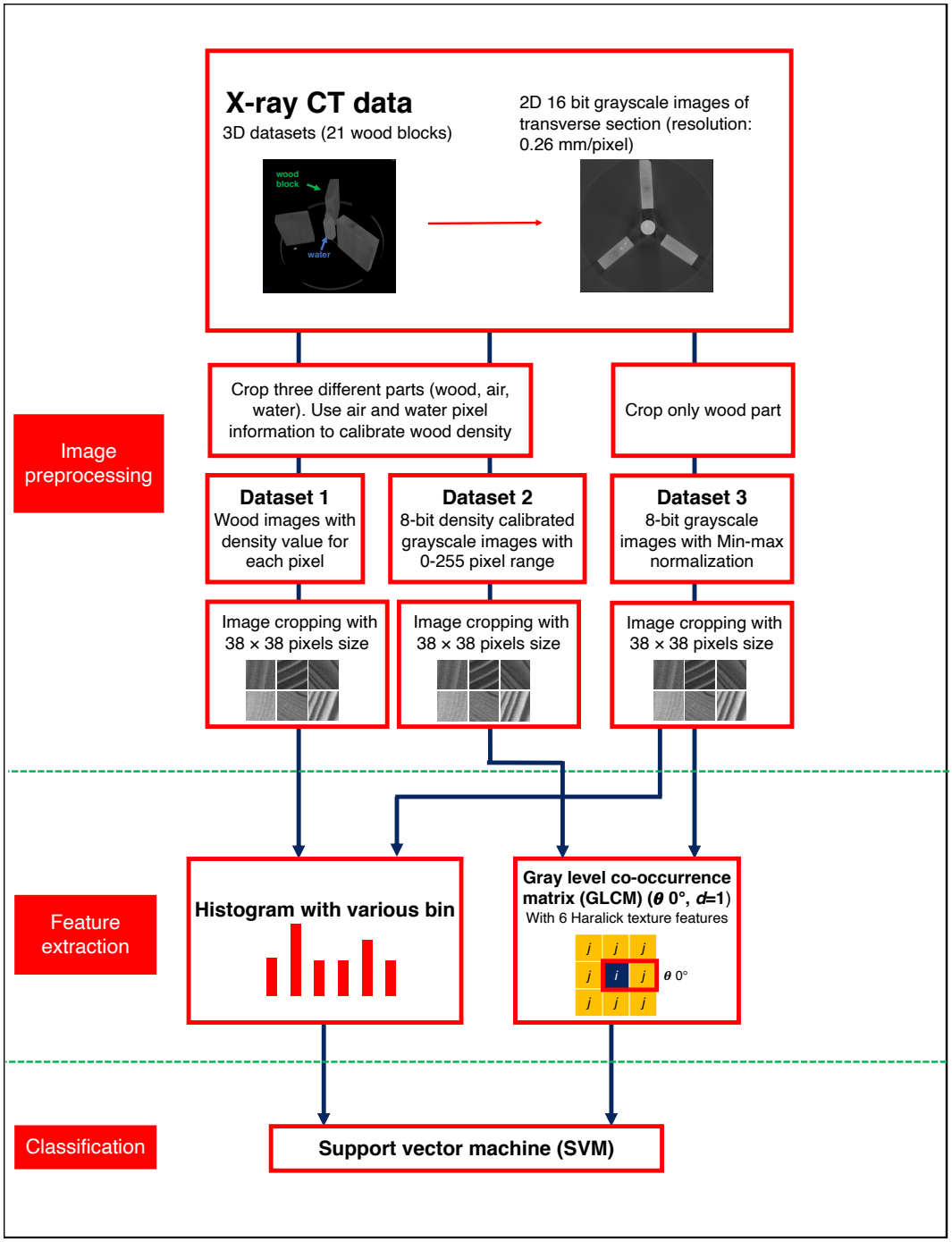

Figure 3.1. Schematic diagram of wood classification method

3.2.3. Image preparation

The volumetric data of reconstructed CT images was consisted of 16-bit grayscale slices. Before performing data analysis, three different datasets were prepared (Figure 3.1):

1. Dataset 1: wood images with density value for each pixel. For dataset 1, density value was calculated by converting gray level value of wood into density by firstly converting gray level of air into 0.0 (density of air), and gray level of water into 1.0 (density of water).
2. Dataset 2: 8-bit calibrated grayscale images with 0-255 pixel range. This dataset was obtained by converting dataset 1 into 0-255 pixel range that corresponds to 0 – 1.2 (density range) (Kobayashi et al., 2019).
3. Dataset 3: 8-bit grayscale images with min-max normalization value of the original images 16-bit grayscale images.

From each dataset, five axial position was selected. A cross section image was extracted from each position. A number of 2D gray-level data of 38×38 pixels (approximately 1 cm×1 cm) were digitally cropped from the five cross-sectional images. Figure 3.2 shows a cross-sectional image of *B. schmidtii*. The cropping process was conducted to obtain as many non-overlapping cropped images as possible. The number of cropped images for each sample was determined by the dimensions of the sample. For example, for *B. schmidtii* (Figure 3.2), it was possible to obtain 56 cropped images from one cross-sectional image. The total for five cross-sectional images was 280 cropped images. Figure 3.3 shows an example of cropped images of each species.

To obtain feature of density histogram, from each species, a set of 12 and 25 bins histogram of density with fixed range of 0.1 – 1.2 g/cm^3 were prepared using the cropped images of dataset 1. Figure 3.4. show that the cropped image of dataset 2 was used to use to generate matrix of GLCM which then processed into six textural features: contrast, dissimilarity, homogeneity, ASM (angular second moment), energy, and correlation (Hall-Beyer, 2017; Haralick et al., 1973).

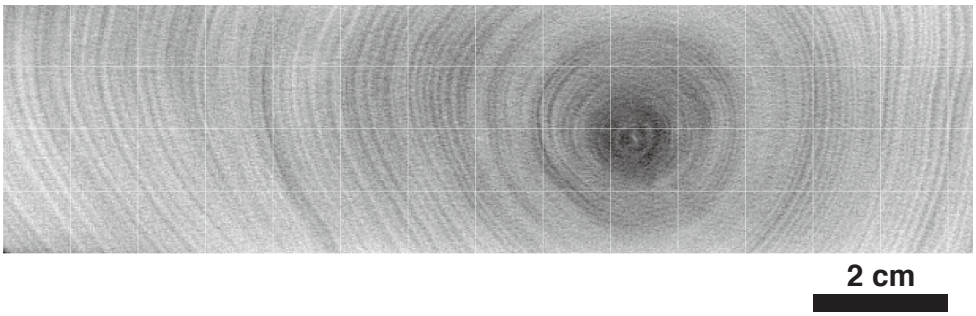

Figure 3.2. One cross-sectional image of *B. schmidtii* was divided into cropped images of 38×38 pixels without overlap, as illustrated by the mesh. The wood also shows a low-density region in the pith region

Meanwhile, for dataset 3, the dataset will represent a data without density information. A set of 12 and 25 bins histogram of grayscale with fixed range of 0-255 for each image. Also, textural features were extracted by generating GLCM and the six textural features from the dataset 3. SVM (support vector machines) was used as classifier. The dataset preparation, feature extraction, and classification processes were implemented using the Python programming language (Python Software Foundation, 2016). To generate GLCM and the extract the textural features, Scikit image libraries were used, which also written in Python (van der Walt et al., 2014).

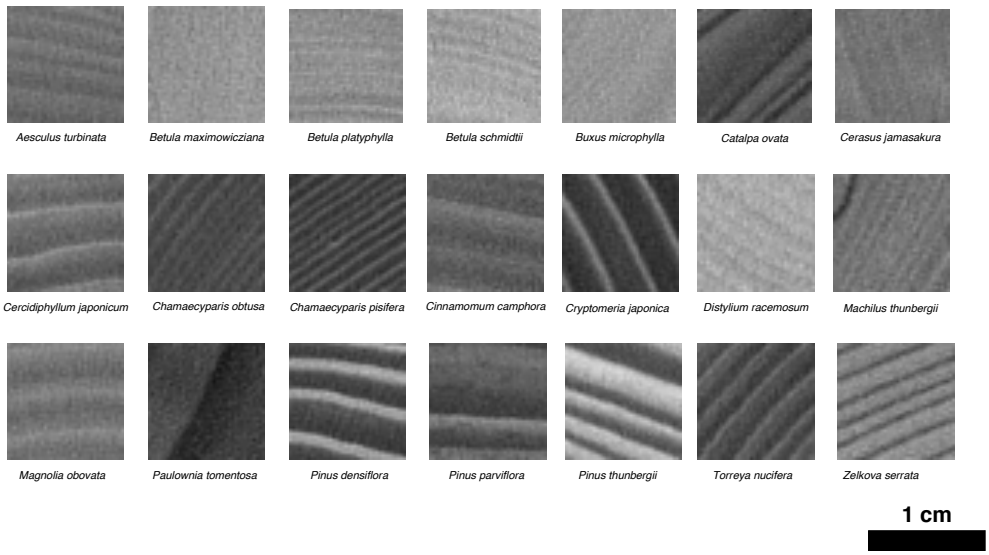

Figure 3.3. Typical cropped cross-section images with a dimension of 38 × 38 pixels

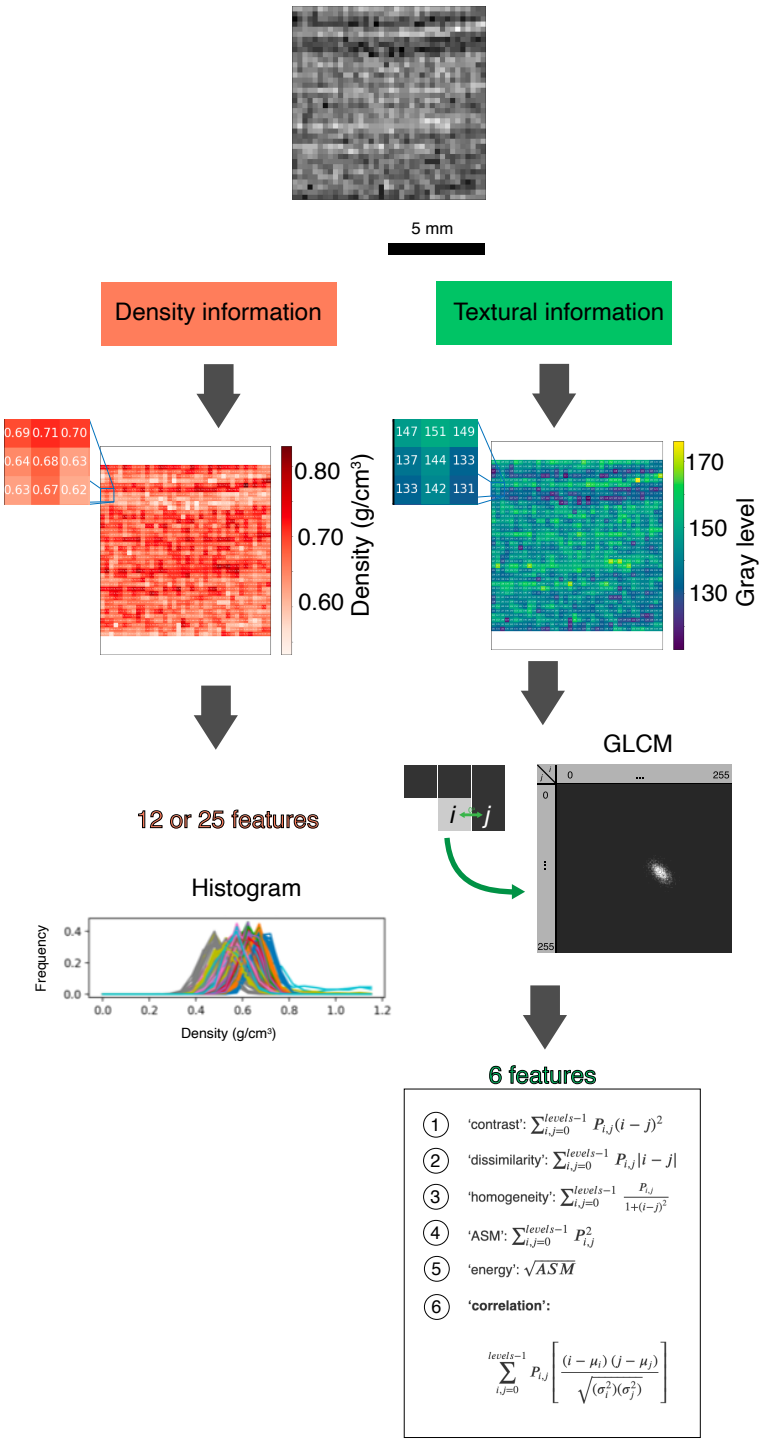

Figure 3.4. Detail of feature extraction process to obtain density information and textural information. Each image with size 38×38 pixel was translated into 12 or 25 features of density information, depend on assigned bin number of histograms. While, each image of the same size was translated into 6 features of textural information by firstly generating GLCM matrix.

3.3. Result and discussion

Wood classification based on density histogram and textural analysis of 21 species that often used to make culturally important wood objects was conducted. CT images of 21 species show limited information of the species' anatomical morphology due to inadequate spatial resolution (Figure 3.2, 3.3). Individual xylem element could not be observed. Therefore, conventional identification procedure will be difficult to carry out. To visualize certain expected features voxel size should be smaller than the expected features (Withers et al., 2021). For example, vessel as a xylem element with larger diameter. The diameter of vessel can be varied, from around 50 – 200 μm (Baas et al., 1983). Voxel resolution 261.5 μm as used in this study was not enough to visualize individual vessel.

Figure 3.3 shows typical cropped wood with dimension of 38 × 38 pixel that almost equal to 1 cm × 1 cm. This dimension was selected based on the condition of real cultural wooden object. For example, the thickness of a Noh mask, which is a wooden mask typically worn in a Japanese traditional theater, may be less than one centimeter. The use of metal foil on the surface of cultural objects (Richter, 2005) can potentially obstruct the observation of wooden components, as metal materials have high X-ray attenuation and can therefore block or absorb the X-rays used for imaging (Lehmann and Mannes, 2012). This can result in a reduction of the visible area of the wooden components on the images obtained through X-ray CT analysis.

Figure 3.4 illustrates the process of translating CT images into features of density from an image of *B. platyphylla* with size 38×38 pixels. To obtain density information, dataset 1 which each pixel contain density value was converted into a one-dimensional histogram. The histogram illustrates the distribution of pixel values in a cropped image. The x-axis represents the range of density or intensity values, depending on the dataset (dataset 1 or dataset 3), while the y-axis indicates the number of pixels that have those values, normalized to a range of 0 to 1. The histogram is composed of bins, with each bin representing a specific value range. In this study, the number of bins was either 12 or 25, and the features were extracted based on the frequency values within each bin. As a result, the number of features depended on the number of bins used.

In addition, Figure 3.4 also illustrate the extraction features of textural information from a cropped image of *B. platyphylla*. The figure shows an image composed of many pixels, which can be represented as a matrix of numbers, with each number representing the intensity of a pixel (Hwang and Sugiyama, 2021). To analyze the texture of an image, it was first converted into a gray level co-occurrence matrix (GLCM). This matrix, denoted as $P(i, j)$, represents the probability of finding a pair of pixels with gray levels i and j at a certain distance from each other (Kobayashi et al., 2015). Figure 3.5 shows examples of GLCM matrices for different species. As different species might have distinctive textures, their GLCM matrices might also differ. To further characterize these textures, six statistical measures (contrast, dissimilarity, homogeneity, ASM, energy, and correlation) were calculated from the GLCM using the equation shown in Figure

3.4. These measures, known as textural features (Hall-Beyer, 2017; Haralick et al., 1973; van der Walt et al., 2014), will be another 6 features that were used for building classification model.

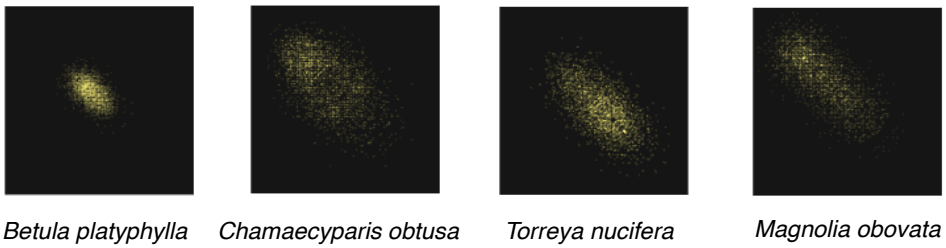

Figure 3.5. Example of GLCM of different species

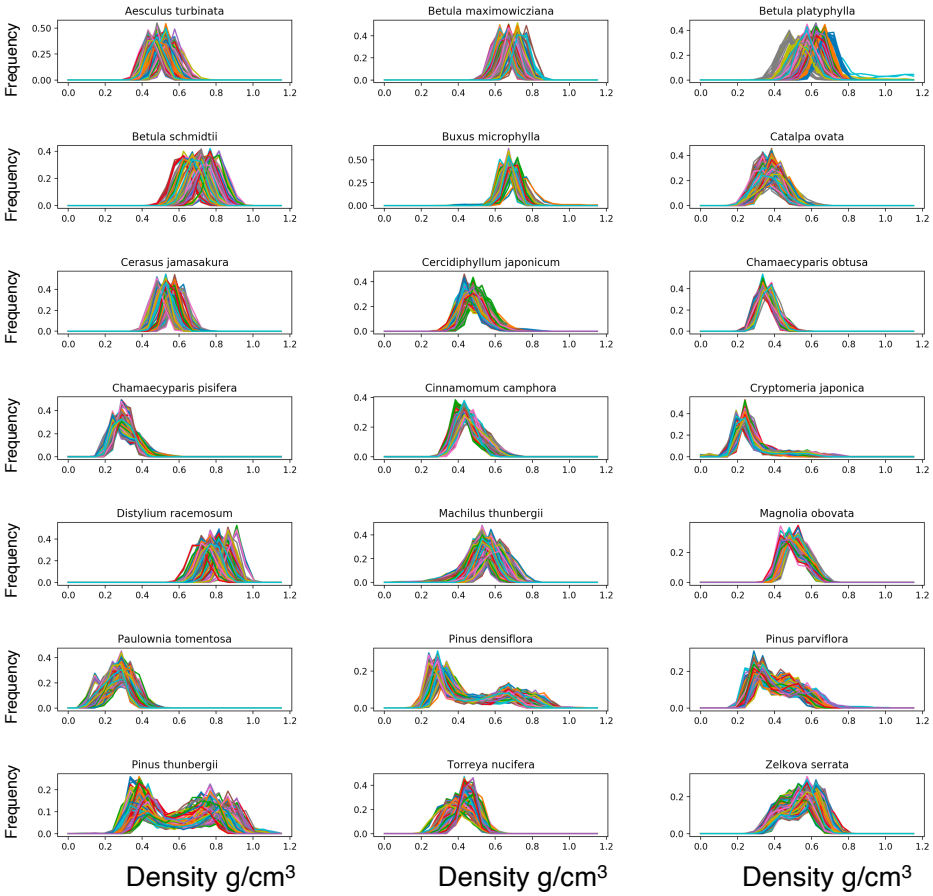

Figure 3.6. Histogram of density values for all cropped images of each species, with 25 bins.

Figure 3.6. shows histogram of density value with 25 bins. The histograms pattern shows one-dimensional data of density value. Some species had distinctive peaks, especially genus *Pinus*: *Pinus densiflora*, *P. thunbergii*, and *P. parviflora.* As seen in Figure 3.3, these tree species had obvious distinct earlywood and latewood. Earlywood is a component of the annual ring that has brighter pixels, and latewood is a part of the annual ring that has darker pixels. Figure 3.6. also show some species had large variation of density variation, i.e. *Aesculus turbinata, Betula platyphylla, B. schmidtii,* and *Distylium racemosum.* The large variation of density histogram, might be caused by heterogeneity of wood material density. For example, in *B. schmidtii* wood block, it contained low density pith area (Figure 3.2).

The prediction accuracy of this study, tested using SVM classifier, is presented in Figure 3.7. Using density information was useful to increase the accuracy of classification model. Wood density variation can reflect anatomical features of wood (De Mil et al., 2018; Zheng and Martínez-Cabrera, 2013). Therefore, incorporate density information into classification model will enhance accuracy of prediction (Kobayashi et al., 2019). The highest accuracy was achieved by combining textural features of GLCM and histogram of calibrated density with 25 bins with accuracy 91.5% (Figure 3.7). Textural GLCM features are commonly used to create wood classification models with X-ray CT image datasets (de Andrade et al., 2020; Hwang and Sugiyama, 2021; Kobayashi et al., 2019, 2017, 2015). In present study, the textural features were useful to increase prediction accuracy. However, using only textural features without density histogram, the prediction accuracy achieved was only 62%. With the ability of X-ray CT to

provide 3D structure of wood, it may be possible to use 3D dataset instead of 2D dataset, as has already been introduced in the medical field and geology (Jardine et al., 2018; Tan et al., 2020).

Figure 3.8 shows confusion matrix that shows accuracy of prediction in species level. The actual wood species are listed on the y-axis, and the predicted wood species are displayed in the columns. Correct predictions of species are presented along the diagonal of the confusion matrix, while incorrect predictions are located elsewhere. The value in each cell indicates the proportion of all predictions that fall into that particular species. The sum of all values in each row is always 1.0. In softwood, a clear difference between earlywood and latewood created noticeable distinction that makes the prediction accuracy of softwood species achieved more than 80%. Meanwhile, it was still found that misclassification occurred on diffuse-porous hardwood. For instance, *B. schmidtii* was often misclassified as *Distylium racemosum*. The difficulty to distinguish these species might be caused similarity of density variation (Figure 3.6). In addition, based on the appearance of cropped images (Figure 3.3.), *B. schmidtii* and *D. racemosum* quite similar with annual rings include in the images.

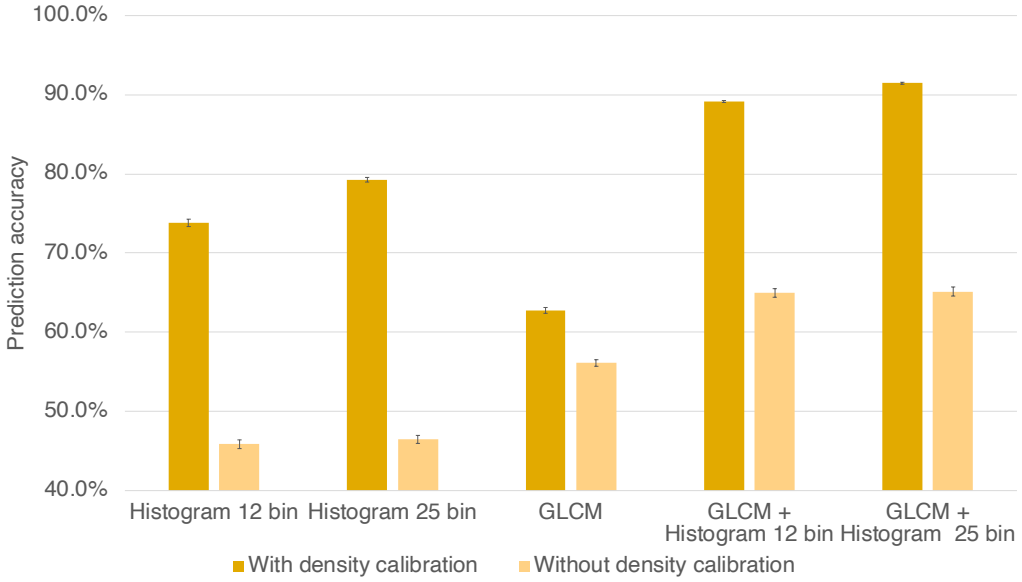

Figure 3.7. Prediction accuracy with and without density calibration. Error bars indicate standard errors (n=10)

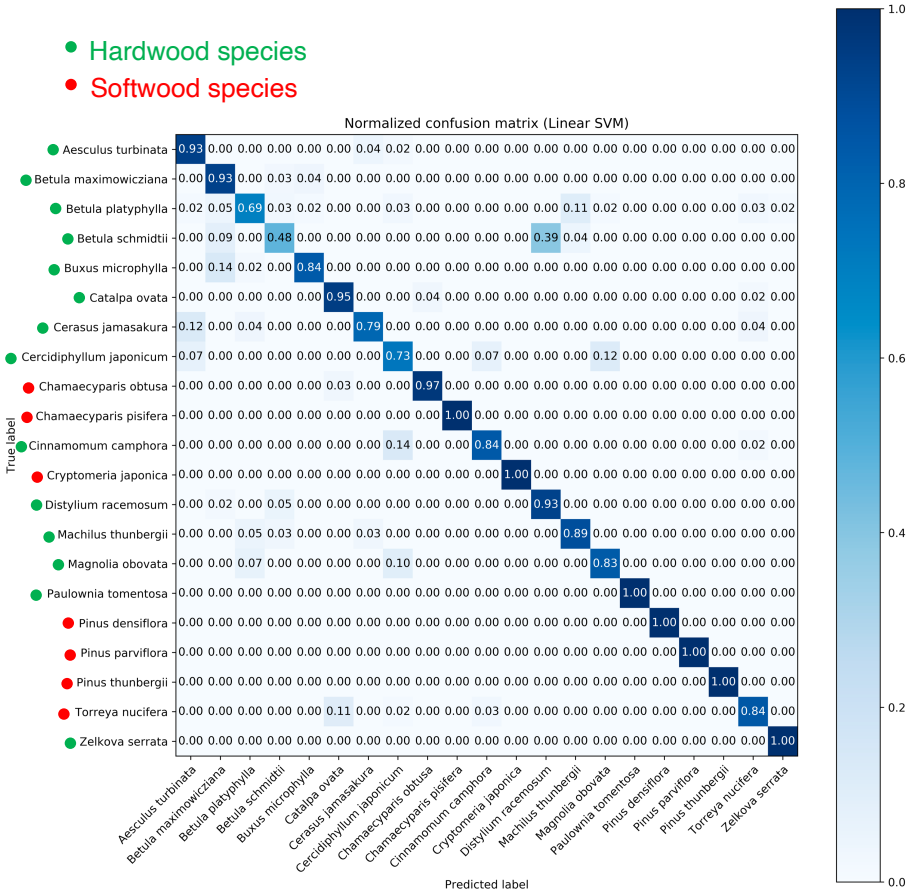

Figure 3.8. Confusion matrix showing prediction accuracy when using combination of calibrated density histogram with bin number 25 and GLCM textural traits as features.

3.4. Summary

X-ray CT was used to visualize 3D structure 21 Japanese wood species that frequently used to build cultural properties in Japan. The dataset of X-ray CT images was used to develop wood classification model by using features generated from histogram of density and textural features of GLCM. The highest prediction accuracy achieved by combining density histogram features and GLCM textural features with accuracy 91.5% using SVM classifier. This study suggests a

possibility to develop an automatic recognition system based on density histogram variation and image textural features to identify species from the CT-images.

Chapter 4 Examination of *Cinnamomum camphora* interlocked grain adopting X-ray computed tomography combined with particle image velocimetry

4.1.Introduction

The wood grain of a living tree is not always straight or parallel to the longitudinal axis of the tree (Harris, 1989). Terms have been used to define the inclined grain depending on the degree of deviation from the longitudinal axis; namely, wavy grain, spiral grain, and interlocked grain (Harris, 1989; Hejnowicz and Romberger, 1979). An interlocked grain occurs when there is a periodic change in the grain angle between left- to right-handed spirals over the course of years (Brémaud et al., 2010; Krawczyszyn, 1972; Krawczyszyn and Romberger, 1980). Such grain deviation affects the woodworking process and physical-mechanical properties of the wood (Coelho et al., 2020; Harris, 1989; Hernandez and Almeida, 2003; Ma et al., 2019).

The interlocked grain of tropical tree species has been reported in numerous studies (Bossu et al., 2018; Brémaud et al., 2010; Hernandez and Almeida, 2003; Koehler, 1931; Kojs et al., 2004; Martley, 1920; Ogata et al., 2003; Ogata and Fujita, 2005). *Cinnamomum camphora ,* which usually grows in temperate and subtropical regions, was observed in the present study (CABI, 2020). The interlocked grain is also found in this species (Oda et al., 2001; Youming et al., 2001). *C. camphora*

wood is selected for making Buddhist images and cabinets in Japan (Mertz, 2011). Unlike the case for tropical species, which have a less clear growth ring boundary, the growth ring boundary of *C. camphora* is annual and distinct because the earlywood vessels appear to be distinctly larger than latewood vessels. Such type of vessel porosity is known as semi-ring porous.

The wood grain orientation is related to the orientation of longitudinal cells that reflect the orientation of parental fusiform cambial cells (Harris, 1989; Hejnowicz and Romberger, 1979; Kitin et al., 2003; Krawczyszyn and Romberger, 1980; Kubler, 1991; Ogata et al., 2003). Therefore, in addition to using the conventional radial splitting method, which is invasive (Hernandez and Almeida, 2003; Krawczyszyn and Romberger, 1980; Martley, 1920), wood grain orientation can be evaluated by examining the orientation of longitudinal cells such as fibers and vessels. Fibers generally account for 30–80% on composition of angiosperm wood, by volume, which will define grain orientation (Spicer, 2016). To see fibers at the cellular level and evaluate grain orientation, serial sectioning on tangential sections is commonly used (Ogata et al., 2003).

Vessels also originate from the same parental cells as fibers. Thus, vessel orientation can also be used as a proxy for grain orientation (Bhat and Bhat, 1983; Brémaud et al., 2010; Collings et al., 2021; Kubler, 1991; Ogata et al., 2003). Although the vessels and fibers have similar orientation, different grain orientations commonly occur in reversal zone of interlocked grain in which vessels run steeper than fibers (Bhat and Bhat, 1983; Collings et al., 2021; Ogata and Fujita, 2005). Unlike fibers, vessels are actually long hollow tubes that can extend from

centimeters to meters in length, that have relatively larger diameters. These vessels are composed of longitudinally aligned series of vessel elements (Spicer, 2016). This structure can be utilized to examine grain orientation. The orientation can be measured by mapping vessels on consecutive transverse sections (Kitin et al., 2004). When vessels are inclined and not parallel to the longitudinal axis of the tree, there is a lateral shift of the vessel between two consecutive transverse sections at different depths. However, serial sectioning technique is time-consuming, requiring training and experience to obtain a satisfactory result. Meanwhile, cross-correlation has been adopted to automatically evaluate the grain angle from such lateral shifting in a pair of transverse images from different depths extracted from a single cross section using a confocal microscope (Ogata and Fujita, 2005). However, this method only works on pair transverse images with narrow depth because of the inadequate intensity of the lower image of the section. Additionally, this method requires sectioning of the sample.

X-ray computed tomography (CT) has been applied in wood science studies in recent decades to observe the spatial organization of xylem, which is usually obtained through time-consuming serial sectioning (Brodersen, 2013). The CT technique allows the virtual cutting of a wood sample simulating microtomy, including obtaining serial transverse sections and other sections from any surface. The technology allows a wider region to be observed in a single image acquisition of the wood sample with relatively faster processing compared to serial sectioning method. It also provides a clear surface because X-ray attenuation addresses the problem of the inadequate intensity of the lower image when adopting confocal

microscopy. In addition, interlocked grain of two African mahogany species (Collings et al., 2021) and spiral grain of radiata pine (Thomas et al., 2022) have been studied recently using high resolution CT. These studies make use of CT technique capacity to reconstruct 3D view of wood at cellular level.

Depending on the equipment, a varied resolution of CT images might be obtained (Stock, 2008). Ideally, the equipment should be selected based on the requirements of the investigation. However, in certain situations, it is not possible to use CT equipment with high resolution imaging. Meanwhile, with lower resolution CT images, it is difficult to visualize wood elements at the cellular level, especially fibers which are important to examine grain orientation. Nevertheless, due to their larger size, vessels can still be observed in lower resolution CT images. For example, Considerably lower resolution CT imaging at 50 micrometers per pixel has been previously used and found to be sufficient for detecting vessels in *C. camphora* (Kobayashi et al., 2015). Therefore, a technique was sought to be developed that could evaluate the orientation based on the appearance of vessels on lower resolution CT images.

Adoption of particle image velocimetry (PIV) was proposed for evaluating the interlocked grain of transverse images of *C. camphora* wood. PIV is often used to study liquid or gas material flow, cell imaging, and cloud motion among other applications (Bengough et al., 2009; Huertas-Tato et al., 2018; Mittelstaedt et al., 2010; Wong and Searson, 2014). In this study, PIV was used to evaluate the grain deviation in pairs of CT images of *C. camphora* transverse sections by tracking the possibility of displacement of vessels and other cells as particle-like objects in

image pairs with different depths. This analysis involves dividing the images into several sub-regions and applying cross-correlation across image pairs (Schlüter et al., 2016). In addition, the two-dimensional fast Fourier transform (2D-FFT) (Collings et al., 2021; Ogata et al., 2003; Ogata and Fujita, 2005) was used to evaluate the interlocked grain in the tangential section. The present study shows the possibility of evaluating the grain orientation from *C. camphora* images recorded using a low-resolution industrial X-ray CT machine by performing image analysis. Estimation the grain angle variation was conducted by applying PIV to transverse sections. The result of the PIV of transverse sections was then validated using the 2D-FFT of tangential sections. Furthermore, this study shows how the variation in the vessel orientation intra-annual ring can be obtained from the PIV output.

4.2.Materials and Methods

4.2.1. Wood material

The wood block of *C. camphora* was similar to a block that was used in a previous study (Kobayashi et al., 2015). The block used in the present study was scanned using an X-ray CT instrument (Y.CT Modular, YXLON International GmbH, Hamburg, Germany) at the Kyushu National Museum. The CT scanning was conducted with a resolution of 0.05 mm per pixel. This process provided projection images, which were then reconstructed into two-dimensional (2D) image slices of the wood block. A volume graphic software (VGStudio MAX 2.2, Volume Graphic GmbH, Heidelberg, Germany) was used to visualize the three-dimensional

(3D) reconstructed volume of *C. camphora* from the slices of 2D images and prepared a suitable image series for analysis.

4.2.2. Pretreatment

Images of a transverse section of the actual wood block were precisely prepared by aligning the volume of reconstructed CT images (Figure 4.1). This process provided a series of transverse images with dimensions of 1433 × 1478 pixels. The images were rotated to align the annual rings in the vertical direction. The images were cropped to 948 × 344 pixels, corresponding to dimensions of 47.4 mm × 17.2 mm.

Other datasets were prepared by extracting oblique transverse sections from a similar volume with the same dimensions as the transverse sections. Two types of oblique transverse section deviating in the tangential direction were prepared. The deviations were 10° in the clockwise direction and 10° in the counterclockwise direction relative to the longitudinal axis of the tree.

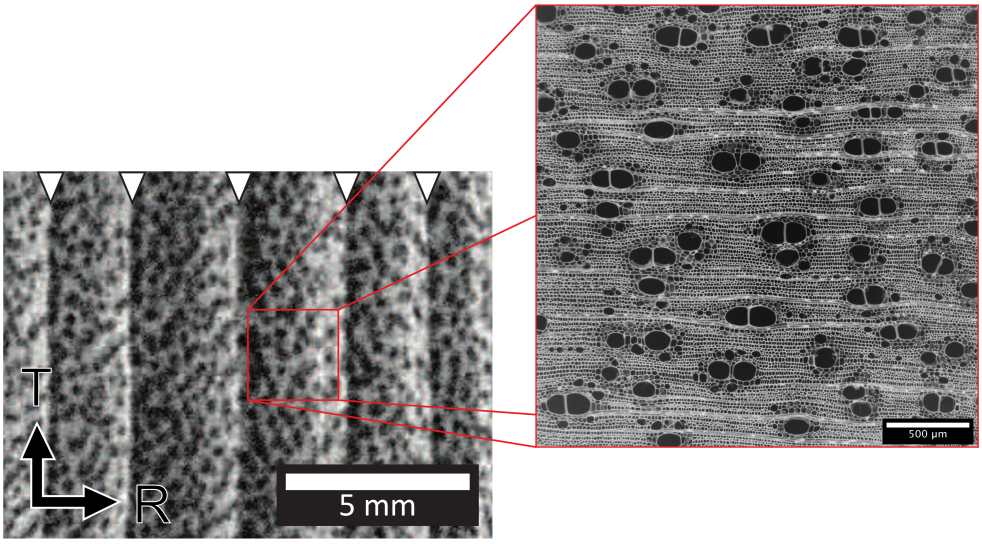

Figure 4.1. Transverse sections of *C. camphora* wood. Left: part of a transverse section of a CT image of *C. camphora* used in the present study. Right: optical microscopy image of *C. camphora* anatomical features for a different specimen. White arrowheads indicate annual ring boundaries. The optical microscopy image (right) is inverted from a brightfield microscopy image to get similar black and white pattern with CT image

Tangential images of the same scale were prepared from a similar volume (Figure 4.2a). A series of tangential images with dimensions of 1433 × 1001 pixels were generated. The images were cropped to 427 × 491 pixels, corresponding to 21.35 mm × 24.55 mm.

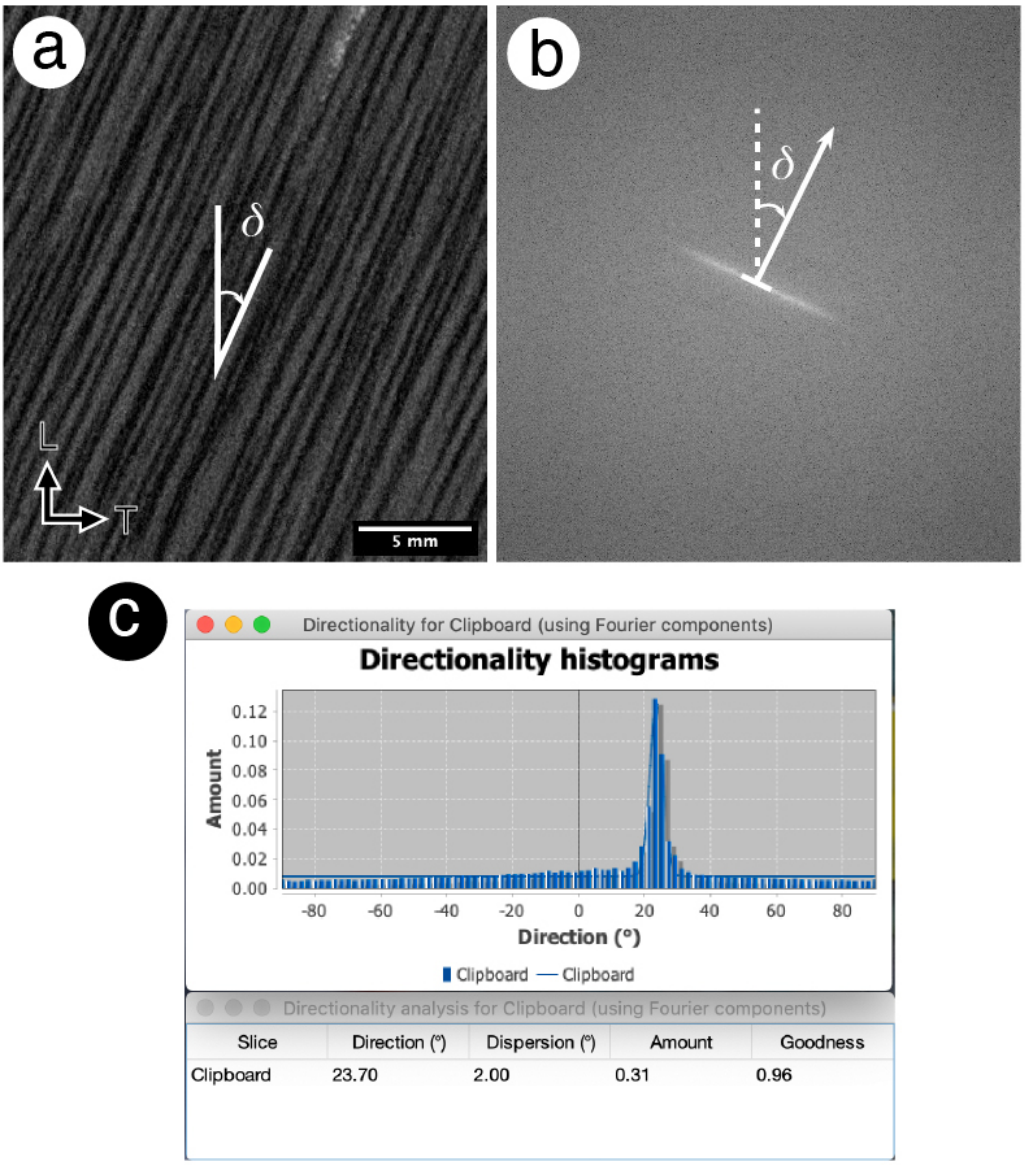

Figure 4.2. An example of measuring the grain angle (δ) in the tangential section of *C. camphora*. **A** Tangential section of CT image showing an estimation of the *C. camphora* grain angle (δ). **B** Power spectrum, calculated using 2D-FFT from **A**, where the arrow indicates the grain angle (δ) measurement. **C** The Directionality plugin's interface shows a histogram, showing the distribution of structures in image **A** according to their orientation, as determined by the power spectrum in **B**. The interface also displays a peak at 23.7°, which indicates the predominant orientation of the structures in the image.

4.2.3. Evaluation of the interlocked grain and vessel network through PIV

To measure interlocked grain, thirty-six sequential transverse images were extracted from the serial transversal images, where images were spaced at intervals of 10 pixels (500 μm). For each image, the next sequential image was its pairing image. A total of 35 pairs of transverse images were thus analyzed in the study. Each pair of images was analyzed adopting PIV. The PIV analysis was programmed in Python (Python Software Foundation, 2016) using the OpenPIV package (Liberzon et al., 2017; Taylor et al., 2010). The program splits each image into sub-regions. These sub-regions are called interrogation windows in the first image and search windows in the second image. A sub-region of 16 × 16 pixels for the interrogation window and a larger sub-region of 32 × 32 pixels for the search window were used in this study. The sub-regions, either interrogation windows or search windows, overlapped each other at a distance of eight pixels from the center of the sub-region.

The PIV program uses cross-correlation and statistical analysis to calculate the displacement of particles or elements between two consecutive images. This is done by applying the fast Fourier transform (FFT) function to windows of the images and comparing their intensity patterns. The program then tracks the most likely displacement of the elements based on the results of this analysis and the assumption that elements within a sub-region of the images correspond to the orientation of the wood grain. This is shown in Figure 4.3. The program also uses statistical analysis to validate the calculated displacement vectors.

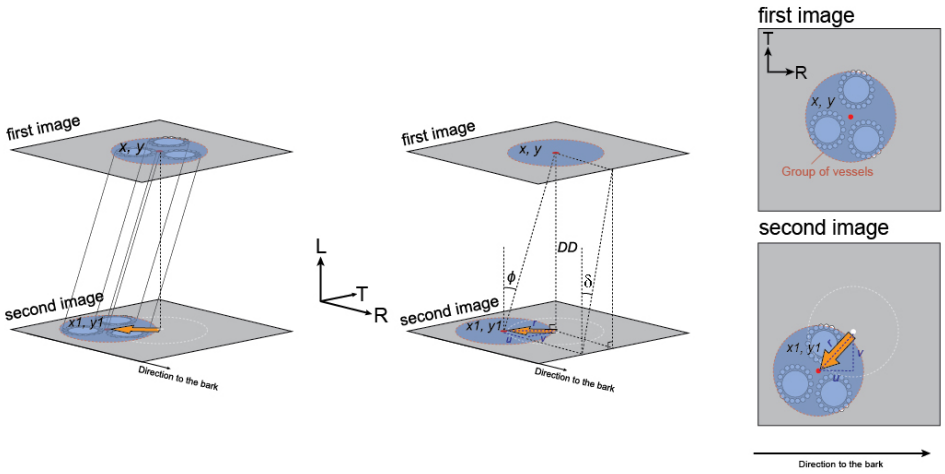

Figure 4.3. Illustration of the lateral shifting of a group of vessels in two consecutive transverse images showing the definitions of the grain angle (δ) and inclination angle (ϕ). Coordinates *x, y* refer to the group of vessels in the first image whereas *x1, y1* refer to the most similar group in the second image. While, *r* is the magnitude of displacement of coordinate *x, y* to *x1, y1*. Wood orthotropic directions: tangential (T), radial (R), and longitudinal (L). Displacement *u* and *v* represent the movement in the radial and tangential direction, respectively.

The output of the image analysis adopting PIV is the coordinates of sub-region vectors (*x, y*) and the vector displacement (*u, v*). Values *u* and *v* correspond to the deviation of the sub-region representing the grain inclination in radial and tangential directions, respectively. The grain angle (δ) was measured according to the displacement of a group of vessels with respect to the axial direction on the tangential plane as seen from the bark side. To obtain the grain angle (δ), an equation proposed by Ogata and Fujita (Ogata and Fujita, 2005) was adapted for examining the grain angle (δ) of *Hopea odorata* Roxb.:

$$\text{grain angle } (\delta) = tan^{-1}\left(\frac{v}{DD}\right), \quad (4.1.)$$

where *DD* is the depth difference in pixels in the longitudinal direction between two consecutive images used for the measurement. A positive value corresponds to right-handed spiral grain and a negative value to left-handed grain. The variation in the radial grain angle obtained from PIV is measured by averaging the grain angle for 35 pairs of transverse images arranged in the longitudinal direction. The value of the grain angle is then also averaged in the tangential direction.

The value of the grain angle (δ) is limited because it only gives the inclination of the grain in the tangential plane. Another calculation from the PIV output was presented, as illustrated in Figure 4.3, to show the displacement vector of grain on a transverse surface representing the grain orientation and the inclination angle (ϕ) at the given orientation. The inclination angle (ϕ) represents the tilt of the grain from the direction of axial growth (Eq. 4.2). To calculate the inclination angle (ϕ), these equations were used:

$$\text{inclination angle } (\phi) = \tan^{-1}\left(\frac{r}{DD}\right), \quad (4.2)$$

$$r = \sqrt{u^2 + v^2}, \quad (4.3)$$

where *r* (Eq. 4.3) is the magnitude of the displacement and *DD* is the depth distance of the virtual sections (Figure 4.3.). The *r* equal to the square root of the sum of the squares of the displacement in the tangential direction (*u*) and the displacement in the radial direction (*v*) (Figure 4.3.).

4.2.4. Interlocked grain analysis using the 2D-FFT

The grain angle (δ) was evaluated from a series of tangential images and 2D-FFT analysis was conducted by measuring the dominant orientation of streaks from

the tangential images. The grain angle (δ) was evaluated from the tangential images automatically using the 2D-FFT algorithm provided in the Directionality plug-in for Fiji (http://fiji.sc/Fiji, Ashburn, VA) (Collings et al., 2021; Liu, 1991; Schindelin et al., 2012). This program generated a power spectrum (Figure 4.2b) with a streak representing the dominant grain orientation from a tangential image (Figure 4.2a). The program then transformed the power spectrum into a histogram. The highest peak in the histogram was used to determine the grain angle (δ) (Figure 4.2c).

4.3.Results and Discussion

4.3.1. Information on the anatomical structure from CT data

The analysis of the interlocked grain applying the PIV and 2D-FFT methods to CT images of *C. camphora* was presented. Figure 4.1 shows the CT image and optical micrograph of *C. camphora* for a transverse section. Compared with the optical micrograph, the CT image with a resolution of 0.05 mm per pixel was unable to reproduce the detailed shape of xylem cells. However, the vessel and surrounding cell lumen distribution were recognizable as dark dots with a diffuse arrangement on the transverse plane. As expected, the differences in density between the vessel lumen and other cell tissue provided contrast sufficient to support further image analysis. Vessels are used as markers because they can be considered as particles in a transverse section for PIV analysis. Annual ring boundary based on radial density variation was also determined (Figure 4.1). Abrupt changes of gray levels from bright to dark, indicating a transition between the end latewood zone into new

earlywood zone, become the boundary between annual rings. Meanwhile, within annual ring, a part with brighter pixel is the earlywood part, and another part with darker pixel is the latewood part. However, the border between earlywood and latewood within annual rings could not be exactly demarcated. Moreover, the vessel network could be seen as dark streaks on tangential planes that undergo periodical changes in orientation along the radial direction (Figure 4.2a). Therefore, in the case of *C. camphora*, vessel elements could be important features in predicting the grain angle (δ) through X-ray CT.

Extracting 2D images from 3D volume CT observations mimics conventional serial sectioning without physically cutting the object. The serial section of the transverse plane of *C. camphora* shows vessels, implying that the continuity of vessel networks could deviate to a certain degree rather than follow a straight course. As seen in the present study, PIV is a useful image analysis tool with which to analyze the existence of interlocked grain in transverse images by tracking the displacement of the vessel network at different depths in the longitudinal direction. Meanwhile, serial sections on the tangential plane explicitly show a periodical change in the grain angle according to the vessel network alignment. Therefore, the 2D-FFT is a suitable option for evaluating the grain angle (δ) as exhibited by the arrangement of longitudinal elements on different tangential surfaces as performed in previous works on *Khaya ivorensis*, *K. senegalensis*, *Hopea odorata* and *Acacia mangium* (Collings et al., 2021; Ogata et al., 2003; Ogata and Fujita, 2005).

The advantage of adopting X-ray CT is that virtual cutting can be performed at any surface position on a wood block. Transverse and tangential sections can be

obtained from a similar CT volume as demonstrated in this study. Other datasets for other sections, such as the oblique transverse section, can be provided. Additionally, the alignment of the section axis, which is usually required when using conventional serial sectioning techniques (Ogata et al., 2003; Ogata and Fujita, 2005), is not necessary. This advantage can increase accuracy and save much time in the observation. Moreover, because CT scanning is a non-invasive and non-destructive technique, it is possible to keep the sample intact for further observation (Kobayashi et al., 2015; Steppe et al., 2004).

4.3.2. Radial variation of the grain angle

Two image analysis methods are presented with which to evaluate the grain angle (δ) of *C. camphora* from CT images (Figure 4.4). Figure 4.4 shows the grain angle (δ) variation evaluated using the two methods, PIV and 2D-FFT, along the radial profile with a distinctive undulation pattern representing fluctuation of the grain angle. The fluctuation might be promoted by the inclination of longitudinal cells toward the tree axis as seen from the bark side, where a positive value represents right-handed spirals and a negative value represents left-handed spirals. The age of the observed region was approximately 22 years according to the number of annual ring boundaries corresponding to peaks in the gray level profile (Figure 4.4). Figure 4.4 shows that there was only one complete period of interlocked grain in the 22 annual rings. One period of interlocked grain means the length between peaks in the same direction (Martley, 1920), which is the 16 years from annual ring $n + 3$ to ring $n + 19$ in this case.

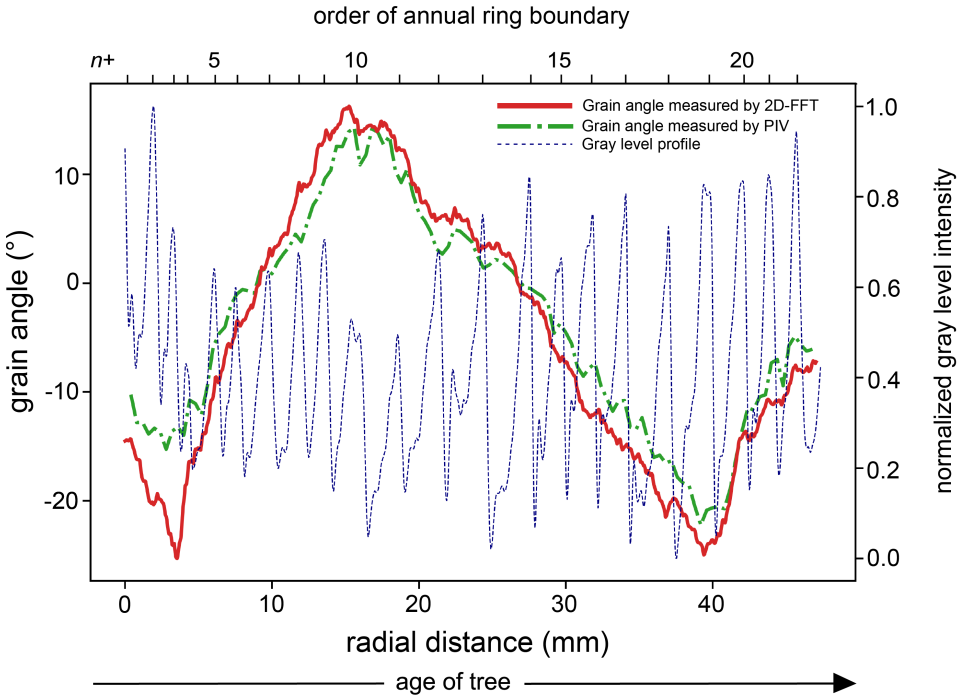

Figure 4.4. Radial variation of the grain angle (δ) measured using PIV and 2D-FFT methods with a positive value indicating right-handed spirals grain and a negative value left-handed spirals grain as seen from the bark side. A dashed blue line represents the gray level profile along the radial direction with higher intensity correlating to higher density. The peaks represent the position of latewood that delineates annual rings.

The radial variations of the grain angle measured using the two methods were similar. The grain angle (δ) of *C. camphora* ranged from −25° to 16° when adopting 2D-FFT based on the serial tangential section and from −22° to 18° when adopting PIV based on transverse sections. In previous work, the maximum amplitude of the *C. camphora* interlocked grain was from 10° to 15° (Oda et al., 2001). Figure 4.4 shows three peaks: two peaks of left-handed grain and one peak of right-handed grain. The first peak was located in growth ring n + 3, the second in n + 10 and the

third in n + 19. Both 2D-FFT and PIV performed well in the analysis of the grain angle variation.

In this study, the maximum grain angle of *C. camphora* was 25° and 22° when measured using the 2D-FFT based on the serial tangential section and PIV based on two transverse sections, respectively. These values were lower than the maximum amplitude of 31° for the tropical species *Bagassa guianensis,* (Bossu et al., 2018) but higher than those for other tropical species (Coelho et al., 2020; Hernandez and Almeida, 2003; Nistal França et al., 2020; Ogata et al., 2003; Ogata and Fujita, 2005; Thinley et al., 2005).

The change in grain angle had a certain intra-annual ring pattern (Figure 4.4). The pattern can be seen in n + 13 annual ring to the n + 19 annual ring. As illustrated in Figure 4.5, near the earlywood, the grain angle changed with constant increment, away from the longitudinal axis. Subsequently, the grain angle increment decreases abruptly and even reverses direction in the earlywood-latewood transition zone heading into the latewood area. This variation may be related to the ability of the vessel to adjust its inclining position rapidly during secondary growth to make contact with adjacent cells (Ogata et al., 2003). Further observation is needed to confirm the intra-annual ring variation with a higher-resolution imaging technique.

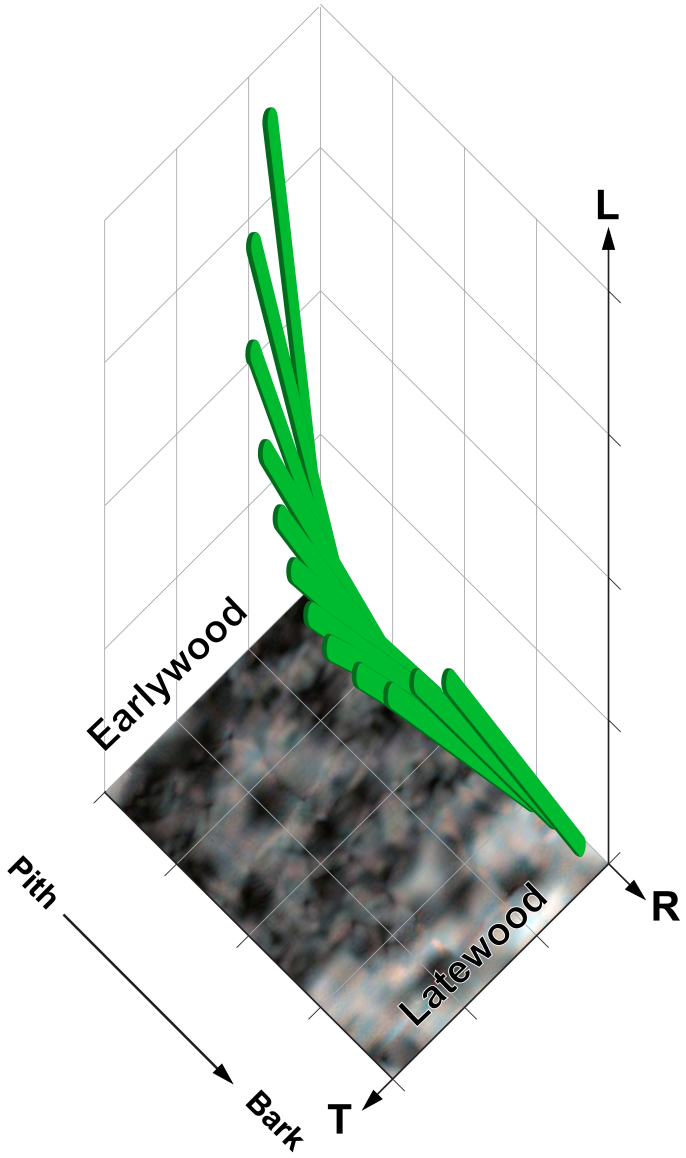

Figure 4.5. Schematic demonstration of localized changes in wood grain within annual ring. Regardless of left- or right-handed grain, grain angle in the middle of annual ring was slightly larger than the angle at the beginning and the end of annual ring. The illustration corresponds to the annual ring of left-handed grain when the grain angle becomes steeper. The trend can be clearly seen in n + 13 annual ring to the n + 19 annual ring. Wood orthotropic directions: tangential (T), radial (R), and longitudinal (L).

4.3.3. Vessel deviation in the transverse sections

The vector plot in Figure 4.6b shows the variation in the grain orientation of *C. camphora* vessels in an example pair of transverse sections (Figure 4.6a) with a depth difference of 500 μm. The arrows in Figure 4.6b show the orientation of the tilted vessel as seen from a transverse view. Most vessels were oriented in a tangential direction (left-handed spiral or right-handed spiral) with high inclination angle. However, the vessels oriented nearly perpendicular to the transverse section (zone 1 and 2 in Figure 4.6b) shows minor orientation that differed from the major orientation. The vessels were inclined towards each other, and some were moving away from each other, following the tangential direction. Some vessels tilted in the radial direction. The same phenomenon also occurred in the oblique transverse sections (Figure 4.7a) that can be observed in zone 1 and 2 (Figure 4.7b) with inclined vessels at 10° in left-handed spirals as well as zone 3, 4, and 5 (Figure 4.7c) with inclined vessels at 10° in right-handed spirals.

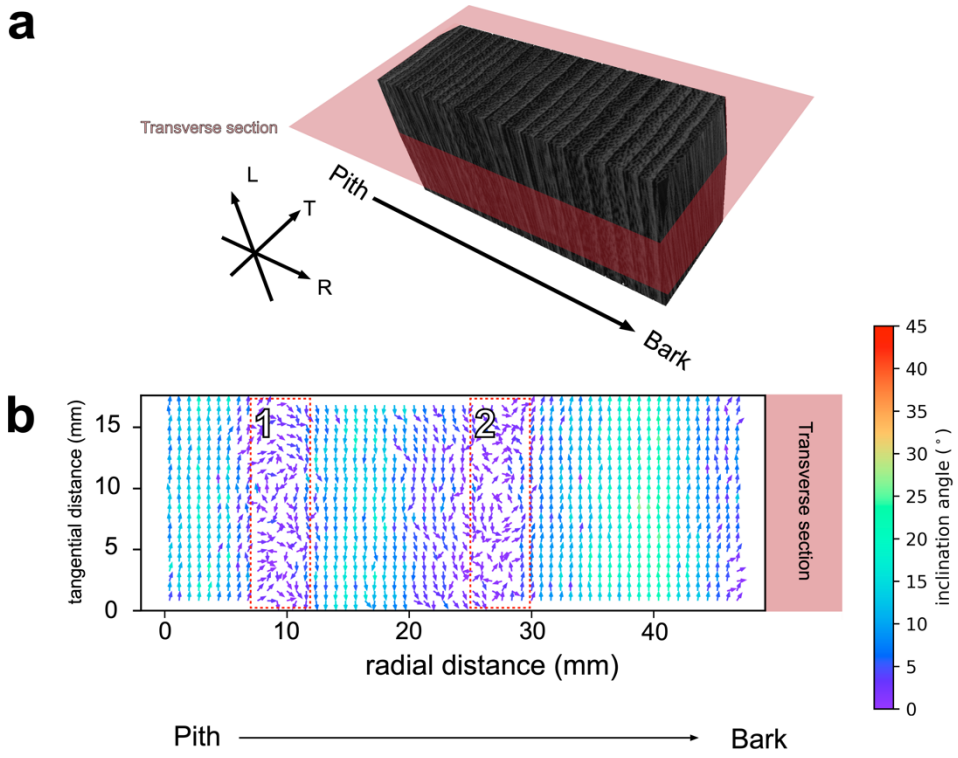

Figure 4.6. Orientation of vessels as seen from transverse sections. **a** Illustration of the transverse section extracted from a *C. camphora* volume. **b** A visualization of the PIV output as a vector field representing the inclining orientation of vessels from an example pair of consecutive transverse images. The arrow color indicates the inclination angle (ϕ) according to the color bar. Zones 1 and 2 are dominated by nearly straight-oriented vessels with an inclination angle 0°–5°. Not all vectors are displayed to avoid overplotting. Wood orthotropic directions: tangential (T), radial (R), and longitudinal (L).

Therefore, such vessel orientations continuously existed along the radial direction from the pith to bark despite the wood grain orientation changing periodically along the radial direction. This phenomenon suggests that the vessels maintain their connection to other cells by inclining at various orientations during

secondary growth. The arrangement might be useful for physiological functions such as water transport in *C. camphora* trees.

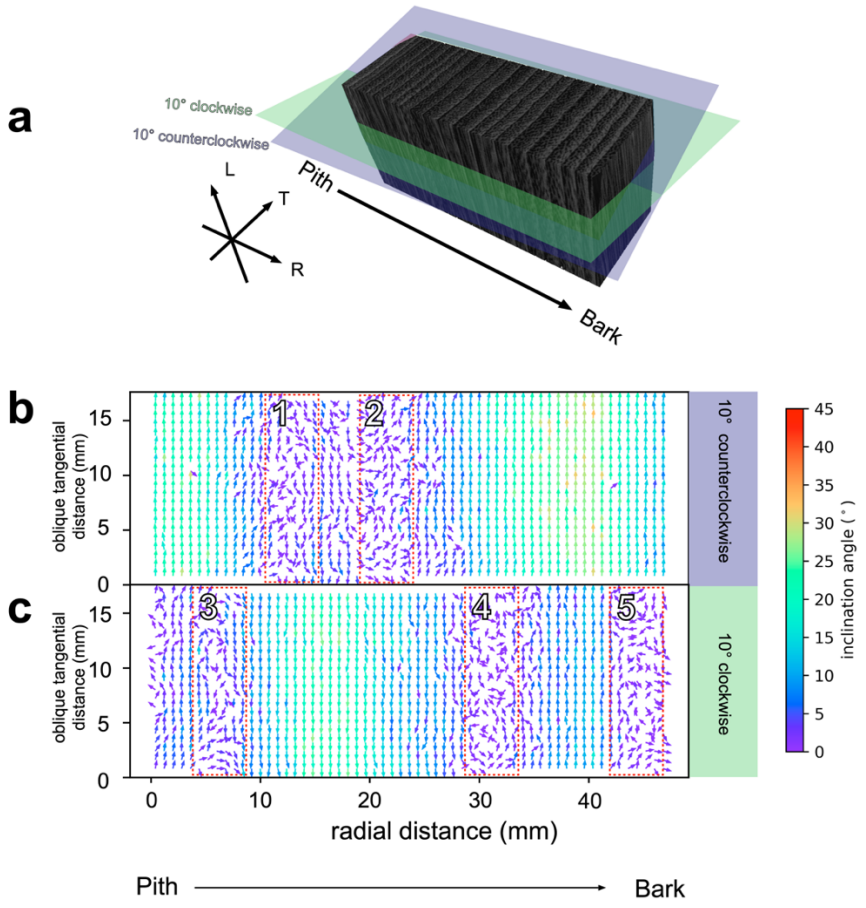

Figure 4.7. Orientation of vessels as seen from oblique transverse sections (10° counterclockwise and 10° clockwise). **a** Illustration of oblique transverse sections extracted from the *C. camphora* volume. Two types of oblique transverse section, with deviations of 10° counterclockwise and 10° clockwise with respect to the longitudinal axis of tree, were extracted from the *C. camphora* volume. Vector field plot showing the PIV output of the oblique transverse section inclined. **b** 10° counterclockwise and **c** 10° clockwise. The arrow color indicates the inclination angle (ϕ) relative to the oblique transverse section axis. Zones 1 and 2 are dominated by vessels with an inclination angle (ϕ) of 10° in left-handed spirals whereas zones 3, 4, and 5 are dominated by vessels with an inclination angle (ϕ) of 10° in right-handed spirals. Not all vectors are displayed to avoid overplotting. Wood orthotropic directions: tangential (T), radial (R), and longitudinal (L).

4.4.Summary

The interlocked grain of semi-diffuse porous hardwood *C. camphora* was evaluated from images obtained using an industrial X-ray CT instrument combined with image analysis. The technique allows obtaining volumetric datasets of wood from which virtual sections can be made from any direction without damaging the samples. Firstly, the grain angle variation from those consecutive transverse images was examined by adopting PIV analysis to track grain displacement. Secondly, 2D-FFT analysis was performed for serial tangential sections of the same datasets. Examination of the grain angle was consistent between the PIV and 2D-FFT, with the maximum amplitude from S to Z spiral being ca. 40°. PIV can also expand our understanding of the minor orientation of vessels of the interlocked grain of *C. camphora*, which is related to the continuity of the vessel network. Such evaluation is important in the examination of mechanical properties as well as hydraulic function in woody plants.

Chapter 5 Conclusions

Wood identification and anatomical investigation using X-ray CT and image analysis has been discussed in this study. As a non-destructive method for visualization of wood structure, X-ray CT is frequently used to inspect designated cultural properties. The purpose of this thesis was to demonstrate the use of X-ray CT to observe wood anatomical characteristics and also identify wood taxa. Standard X-ray CT and SRX-ray μCT were used in this study.

In chapter 1, the importance of wood anatomy and research background is discussed. In addition, introduction of X-ray computed tomography and its importance for wood analysis.

In chapter 2, The use of synchrotron X-ray microtomography (SRX-ray μCT) for identification of Indonesian kris sheath was discussed. Kris is one of traditional dagger from Indonesia. Wood is often used as material for kris sheath. Seven kris sheaths were investigated using SRX-ray μCT. Small size of samples was observed. Then, identification based on anatomical and morphological characteristics was performed. Three taxa were successfully identified which were *Dysoxylum* spp., *Tamarindus indica*, and *Kleinhovia hospita.* The spatial distribution of the prismatic crystals inside the *T. indica* and *K. hospita* xylem cells was also visualized. Abundant crystals were present in *T. indica* arranged in longitudinal alignment inside the chambered axial parenchyma cells. The crystals were arranged in radial alignment inside the ray cells of *K. hospita*. The existence of abundant crystals in series may be important for the mechanical support of certain xylem cells.

In chapter 3, standard X-ray CT with lower spatial resolution was used to classify wood materials often used to make designated cultural properties in Japan. Visualization of 3D structure 21 Japanese wood species frequently used to build cultural properties in Japan was conducted. Then, the dataset of X-ray CT images was used to develop wood classification model by using features generated from histogram of density and textural features of GLCM. The highest prediction accuracy was achieved by combining density histogram features and GLCM textural features with an accuracy of 91.5%.

Finally, in Chapter 4, examination of interlocked grain of *Cinnamomum* was conducted by using standard X-ray computed tomography. The result shows possibility of image analysis to measure and evaluate interlocked grain. Two-dimensional FFT and PIV technique were used to evaluate grain angle variation on *C. camphora*. Periodical changes in the wood grain orientation as left- and right-handed spirals ranging from $-25°$ to $16°$ and $-22°$ to $18°$ using the 2D-FFT and PIV, respectively. Furthermore, despite the major orientation of vessels inclining in the tangential direction, the PIV result revealed a minor deviation with vessels inclining in various orientations along the tree radius.

In conclusion, using standard X-ray computed tomography can be useful to inspect internal structure of wood that can be applied in wood anatomy observation and also wood identification. SRX-ray μCT can be useful to perform microscopic identification due to the high-resolution advantage, even with small amount of sample. As a non-destructive technique, standard X-ray CT can be alternative to perform wood identification of designated cultural properties by adopting computer

vision to extract important species-specific features. Furthermore, with the ability to inspect internal structure object, standard X-ray CT can mimic conventional serial sectioning to reveal 3D organization of wood.

References

Abe, H., 2016. Wood identification research and its importance. Mokuzai Gakkaishi 62, 240–249. (in Japanese)

Araki T., 2020. X-ray CT survey for cultural properties. J. Jpn. Soc. Precis. Eng. 86, 323–327. https://doi.org/10.2493/jjspe.86.323. (in Japanese)

Arifin, M.T., 2006. Keris Jawa: Bilah, Latar Sejarah Hingga Pasar [Javanese kris: blade, historical background to market]. Hajied Pustaka, Jakarta.

Baas, P., Werker, E., Fahn, A., 1983. Some ecological trends in vessel characters. IAWA J. 4, 141–159. https://doi.org/10.1163/22941932-90000407

Beaulieu, J., Dutilleul, P., 2019. Applications of computed tomography (CT) scanning technology in forest research: a timely update and review. Can. J. For. Res. 49, 1173–1188. https://doi.org/10.1139/cjfr-2018-0537

Bengough, A.G., Hans, J., Bransby, M.F., Valentine, T.A., 2009. PIV as a method for quantifying root cell growth and particle displacement in confocal images. Microsc. Res. Tech. 73, 27–36. https://doi.org/10.1002/jemt.20749

Bhat, K.V., Bhat, K.M., 1983. Anatomical changes associated with interlocked grain in *Anacardium occidentale* L. IAWA J. 4, 179–182. https://doi.org/10.1163/22941932-90000410

Bossu, J., Lehnebach, R., Corn, S., Regazzi, A., Beauchêne, J., Clair, B., 2018. Interlocked grain and density patterns in *Bagassa guianensis*: changes with ontogeny and mechanical consequences for trees. Trees 32, 1643–1655. https://doi.org/10.1007/s00468-018-1740-x

Brémaud, I., Cabrolier, P., Gril, J., Clair, B., Gérard, J., Minato, K., Thibaut, B., 2010. Identification of anisotropic vibrational properties of Padauk wood with interlocked grain. Wood Sci. Technol. 44, 355–367. https://doi.org/10.1007/s00226-010-0348-0

Brodersen, C.R., 2013. Visualizing wood anatomy in three dimensions with high-resolution X-ray micro-tomography (μCT) – a review –. IAWA J. 34, 408–424. https://doi.org/10.1163/22941932-00000033

CABI, 2020. *Cinnamomum camphora* (camphor laurel) in Forestry Compendium. CAB International, Wallingford.

Carlquist, S.J., 2010. Comparative wood anatomy: systematic, ecological, and evolutionary aspects of dicotyledon wood, 2., completely rev. ed., softcover version of original hardcover edition 2001. ed, Springer series in wood science. Springer, Berlin.

Casali, F., 2006. Chapter 2 X-ray and neutron digital radiography and computed tomography for cultural heritage, in: Physical Techniques in the Study of Art, Archaeology and Cultural Heritage. Elsevier, pp. 41–123. https://doi.org/10.1016/S1871-1731(06)80003-5

Chappard, C., Basillais, A., Benhamou, L., Bonassie, A., Brunet-Imbault, B., Bonnet, N., Peyrin, F., 2006. Comparison of synchrotron radiation and conventional x-ray microcomputed tomography for assessing trabecular bone microarchitecture of human femoral heads: Bone microarchitecture

from synchrotron radiation and conventional x-ray. Med. Phys. 33, 3568–3577. https://doi.org/10.1118/1.2256069

Coelho, J.C.F., Vidaurre, G.B., da Silva, J.G.M., de Almeida, M.N.F., Oliveira, R.F., Segundinho, P.G. de A., Alves, R.C., Hein, P.R.G., 2020. Wood grain angles variations in *Eucalyptus* and their relationships to physical-mechanical properties. Holzforschung 74, 1089–1097. https://doi.org/10.1515/hf-2019-0131

Collings, D.A., Thomas, J., Dijkstra, S.M., Harrington, J.J., 2021. The formation of interlocked grain in African mahogany (*Khaya* spp.) analysed by X-ray computed microtomography. Tree Physiol. 41, 1542–1557. https://doi.org/10.1093/treephys/tpab020

de Andrade, B.G., Basso, V.M., de Figueiredo Latorraca, J.V., 2020. Machine vision for field-level wood identification. IAWA J. 41, 681–698. https://doi.org/10.1163/22941932-bja10001

De Mil, T., Tarelkin, Y., Hahn, S., Hubau, W., Deklerck, V., Debeir, O., Van Acker, J., de Cannière, C., Beeckman, H., Van den Bulcke, J., 2018. Wood density profiles and their corresponding tissue fractions in tropical Angiosperm trees. Forests 9, 763. https://doi.org/10.3390/f9120763

Donaldson, L., 2008. Microfibril Angle: measurement, variation and relationships – a Review. IAWA J. 29, 345–386. https://doi.org/10.1163/22941932-90000192

Donaldson, L., Nanayakkara, B., Harrington, J., 2017. Wood growth and development, in: Encyclopedia of Applied Plant Sciences. Elsevier, pp. 203–210. https://doi.org/10.1016/B978-0-12-394807-6.00114-3

Fioravanti, M., Di Giulio, G., Signorini, G., 2017. A non-invasive approach to identifying wood species in historical musical instruments. J. Cult. Herit. 27, S70–S77. https://doi.org/10.1016/j.culher.2016.05.012

Franceschi, V.R., Horner, H.T., 1980. Calcium oxalate crystals in plants. Bot. Rev. 46, 361–427. https://doi.org/10.1007/BF02860532

Franceschi, V.R., Nakata, P.A., 2005. Calcium oxalate in plants: formation and function. Annu. Rev. Plant Biol. 56, 41–71. https://doi.org/10.1146/annurev.arplant.56.032604.144106

Frey, E., 2003. The Kris Mystic Weapon of The Malay World, Images of Asia. Institut Terjemahan Negara Malaysia, Kuala Lumpur.

Giachi, G., Guidotti, M.C., Lazzeri, S., Sozzi, L., Macchioni, N., 2016. Wood identification of the headrests from the collection of the Egyptian Museum in Florence. J. Archaeol. Sci. Rep. 9, 340–346. https://doi.org/10.1016/j.jasrep.2016.08.027

Guilley, E., Mothe, F., Nepveu, G., 2002. A procedure based on conditional probabilities to estimate proportions and densities of tissues from X-ray images of *Quercus petraea* samples. IAWA J. 23, 235–252. https://doi.org/10.1163/22941932-90000301

Hall-Beyer, M., 2017. GLCM Texture: A Tutorial v. 3.0 March 2017. https://doi.org/10.11575/PRISM/33280

Haralick, R.M., Shanmugam, K., Dinstein, I., 1973. Textural features for image classification. IEEE Trans. Syst. Man Cybern. SMC-3, 610–621. https://doi.org/10.1109/TSMC.1973.4309314

Harris, J.M., 1989. Spiral Grain and Wave Phenomena in Wood Formation, Springer Series in Wood Science. Springer Berlin Heidelberg, Berlin, Heidelberg. https://doi.org/10.1007/978-3-642-73779-4

Harsrinuksmo, B., 2004. Ensiklopedi keris [Kris encyclopedia]. Gramedia Pustaka Utama, Jakarta.

Haryoguritno, H., 2006. Keris Jawa: antara mistik dan nalar [Javanese kris: between mysticism and logic]. Indonesia Kebanggaanku, Jakarta.

He, T., Lu, Y., Jiao, L., Zhang, Y., Jiang, X., Yin, Y., 2020. Developing deep learning models to automate rosewood tree species identification for CITES designation and implementation. Holzforschung 74, 1123–1133. https://doi.org/10.1515/hf-2020-0006

Heady, R.D., Peters, G.N., Evans, P.D., 2010. Identification of the woods used to make the Riley Cabinet. IAWA J. 31, 385–397. https://doi.org/10.1163/22941932-90000031

Hejnowicz, Z., Romberger, J.A., 1979. The common basis of wood grain figures is the systematically changing orientation of cambial fusiform cells. Wood Sci. Technol. 13, 89–96. https://doi.org/10.1007/BF00368602

Helmling, S., Olbrich, A., Tepe, L., Koch, G., 2016. Qualitative and quantitative characteristics of macerated vessels of 23 mixed tropical hardwood (MTH) species: a data collection for the identification of wood species in pulp and paper. Holzforschung 70, 839–844. https://doi.org/10.1515/hf-2015-0195

Hernandez, R.E., Almeida, G., 2003. Effects of wood density and interlocked grain on the shear strength of three Amazonian tropical hardwoods. Wood Fiber Sci. 35, 154–166.

Hoadley, R.B., 1990. Identifying wood: accurate results with simple tools. Taunton Press.

Hudgins, J.W., Krekling, T., Franceschi, V.R., 2003. Distribution of calcium oxalate crystals in the secondary phloem of conifers: a constitutive defense mechanism? New Phytol. 159, 677–690. https://doi.org/10.1046/j.1469-8137.2003.00839.x

Huertas-Tato, J., Aler, R., Rodríguez-Benítez, F.J., Arbizu-Barrena, C., Pozo-Vázquez, D., Galván, I.M., 2018. Predicting global irradiance combining forecasting models through machine learning, in: de Cos Juez, F.J., Villar, J.R., de la Cal, E.A., Herrero, Á., Quintián, H., Sáez, J.A., Corchado, E. (Eds.), Hybrid Artificial Intelligent Systems. Springer International Publishing, Cham, pp. 622–633. https://doi.org/10.1007/978-3-319-92639-1_52

Hwang, S.-W., Sugiyama, J., 2021. Computer vision-based wood identification and its expansion and contribution potentials in wood science: A review. Plant Methods 17, 47. https://doi.org/10.1186/s13007-021-00746-1

IAWA Committee, 2016. IAWA List of Microscopic Bark Features. IAWA J. 37, 517–615. https://doi.org/10.1163/22941932-20160151

IAWA Committee, 2004. lAWA List of Microscopic Features for Softwood Identification. IAWA Joumal 25, 1–70.
IAWA Committee, 1989. IAWA List of Microscopic Features for Hardwood Identification. IAWA Bull N S 10, 219–332.
Ilvessalo-Pfäffli, M.-S., 2010. Fiber atlas: identification of papermaking fibers, Softcover reprint of the hardcover 1st edition 1995. ed, Springer Series in Wood Science. Springer, Berlin.
InsideWood, 2004. http://insidewood.lib.ncsu.edu.
Jardine, M.A., Miller, J.A., Becker, M., 2018. Coupled X-ray computed tomography and grey level co-occurrence matrices as a method for quantification of mineralogy and texture in 3D. Comput. Geosci. 111, 105–117. https://doi.org/10.1016/j.cageo.2017.11.005
Kaneko, H., Iwasa, M., Noshiro, S., Fujii, T., 2010. Wood types and material selection for Japanese wooden statues of the ancient period, III: further thoughts on 8th- and 9th-century sculptures (in Japanese). Museum 625, 61–78. (in Japanese)
Kaneko, H., Noshiro, S., Abe, H., Fujii, T., Iwasa, M., 2019. Reexamination of "Samples formerly owned by Kohara Jiro for a materials study of wooden sculptures." Museum 679, 5–60. (in Japanese)
Kitin, P., Funada, R., Sano, Y., 2003. Three-dimensional imaging and analysis of differentiating secondary xylem by confocal microscopy. IAWA J. 24, 211–222. https://doi.org/10.1163/22941932-90001590
Kitin, P.B., Fujii, T., Abe, H., Funada, R., 2004. Anatomy of the vessel network within and between tree rings of *Fraxinus lanuginosa* (Oleaceae). Am. J. Bot. 91, 779–788. https://doi.org/10.3732/ajb.91.6.779
Kobayashi, K., Akada, M., Torigoe, T., Imazu, S., Sugiyama, J., 2015. Automated recognition of wood used in traditional Japanese sculptures by texture analysis of their low-resolution computed tomography data. J. Wood Sci. 61, 630–640. https://doi.org/10.1007/s10086-015-1507-6
Kobayashi, K., Hwang, S.-W., Lee, W.-H., Sugiyama, J., 2017. Texture analysis of stereograms of diffuse-porous hardwood: identification of wood species used in Tripitaka Koreana. J. Wood Sci. 63, 322–330. https://doi.org/10.1007/s10086-017-1625-4
Kobayashi, K., Hwang, S.-W., Okochi, T., Lee, W.-H., Sugiyama, J., 2019. Non-destructive method for wood identification using conventional X-ray computed tomography data. J. Cult. Herit. 38, 88–93. https://doi.org/10.1016/j.culher.2019.02.001
Koehler, A., 1931. More about twisted grain in trees. Science 73, 477–477. (in Japanese). https://doi.org/10.1126/science.73.1896.477
Kohara, J., 1972. Ki no bunka [The culture of wood]. Kashima syuppankai, Tokyo. (in Japanese)
Kohara, J., 1964. Nihon chōkoku yōzai chōsa shiryō [The data on the investigation of the material used for Japanese sculptures]. Bijutsu Kenkyū 229, 32–41. (in Japanese)
Kojs, P., Włoch, W., Rusin, A., 2004. Rearrangement of cells in storeyed cambium of *Lonchocarpus sericeus* (Poir.) DC connected with formation of

interlocked grain in the xylem. Trees 18, 136–144. https://doi.org/10.1007/s00468-003-0292-9
Krawczyszyn, J., 1972. Movement of the cambial domain pattern and mechanism of formation of interlocked grain in *Platanus*. Acta Soc. Bot. Pol. 41, 443–461. https://doi.org/10.5586/asbp.1972.036
Krawczyszyn, J., Romberger, J.A., 1980. Interlocked grain, cambial domains, Endogenous rhythms, and time relations, with emphasis on *Nyssa sylvatica*. Am. J. Bot. 67, 228–236. https://doi.org/10.1002/j.1537-2197.1980.tb07646.x
Kubler, H., 1991. Function of spiral grain in trees. Trees 5, 125–135. https://doi.org/10.1007/BF00204333
Landis, E.N., Keane, D.T., 2010. X-ray microtomography. Mater. Charact. 61, 1305–1316. https://doi.org/10.1016/j.matchar.2010.09.012
Lehmann, E.H., Mannes, D., 2012. Wood investigations by means of radiation transmission techniques. J. Cult. Herit. 13, S35–S43. https://doi.org/10.1016/j.culher.2012.03.017
Leonardon, M., Altaner, C.M., Vihermaa, L., Jarvis, M.C., 2010. Wood shrinkage: influence of anatomy, cell wall architecture, chemical composition and cambial age. Eur. J. Wood Wood Prod. 68, 87–94. https://doi.org/10.1007/s00107-009-0355-8
Liberzon, A., Lasagna, D., Aubert, M., Bachant, P., Jakirkham, Ranleu, Borg, J., Dallas, C., 2017. Openpiv/Openpiv-Python: Bug fixes from 0.20.8 due to Python 3 division and from range(0,0) to range(0,1).
Liu, S., He, T., Wang, J., Chen, J., Guo, J., Jiang, X., Wiedenhoeft, A.C., Yin, Y., 2022. Can quantitative wood anatomy data coupled with machine learning analysis discriminate CITES species from their look-alikes? Wood Sci. Technol. 56, 1567–1583. https://doi.org/10.1007/s00226-022-01404-y
Liu, Z.-Q., 1991. Scale space approach to directional analysis of images. Appl. Opt. 30, 1369. https://doi.org/10.1364/AO.30.001369
Ma, T., Inagaki, T., Tsuchikawa, S., 2019. Three-dimensional grain angle measurement of softwood (Hinoki cypress) using near infrared spatially and spectrally resolved imaging (NIR-SSRI). Holzforschung 73, 817–826. https://doi.org/10.1515/hf-2018-0273
Martley, J.F., 1920. Double cross-grain. Ann. Appl. Biol. 7, 224–268. https://doi.org/10.1111/j.1744-7348.1920.tb05309.x
Mertz, M., 2011. Wood and Traditional Woodworking in Japan. Kaiseisha Press.
Mittelstaedt, E., Davaille, A., van Keken, P.E., Gracias, N., Escartin, J., 2010. A noninvasive method for measuring the velocity of diffuse hydrothermal flow by tracking moving refractive index anomalies. Geochem. Geophys. Geosystems 11, Q10005. https://doi.org/10.1029/2010GC003227
Mizuno, S., Torizu, R., Sugiyama, J., 2010. Wood identification of a wooden mask using synchrotron X-ray microtomography. J. Archaeol. Sci. 37, 2842–2845. https://doi.org/10.1016/j.jas.2010.06.022
Moebirman, 1973. Keris and other weapons of Indonesia. Yayasan Pelita Wisata, Jakarta.

Nečemer, M., Lazar, T., Šmit, Ž., Kump, P., Žužek, B., 2013. Study of the Provenance and Technology of Asian Kris Daggers by Application of X-ray Analytical Techniques and Hardness Testing. Acta Chim Slov 60, 351–357.

Nilsson, T., Rowell, R., 2012. Historical wood – structure and properties. J. Cult. Herit. 13, S5–S9. https://doi.org/10.1016/j.culher.2012.03.016

Nistal França, F.J., Filgueira Amorim França, T.S., Vidaurre, G.B., 2020. Effect of growth stress and interlocked grain on splitting of seven different hybrid clones of *Eucalyptus* grandis×*Eucalyptus urophylla* wood. Holzforschung 74, 917–926. https://doi.org/10.1515/hf-2019-0209

Oda, K., Oishi, M., Ogata, S., Matsumura, J., 2001. Formation and significance of interlocked grain in *Cinnamomum camphora I*. Bull. Kyushu Univ. For. 82, 11–20. (in Japanese)

Ogata, K., Fujii, T., Abe, H., Baas, P., 2008. Identification of the timbers of Southeast Asia and the Western Pacific. Kaiseisha Press, Otsu.

Ogata, Y., Fujita, M., 2005. New anatomical method of grain angles measurement using confocal microscopy and image cross-correlation. Trees 19, 73–80. https://doi.org/10.1007/s00468-004-0365-4

Ogata, Y., Fujita, M., Nobuchi, T., Sahri, M.H., 2003. Macroscopic and anatomical investigation of interlocked grain *Acacia mangium*. IAWA J. 24, 13–26. https://doi.org/10.1163/22941932-90000317

Python Software Foundation, 2016. Python Version 3.5.2.

Ramos, A.C., Regan, S., 2018. Cell differentiation in the vascular cambium: new tool, 120-year debate. J. Exp. Bot. 69, 4231–4233. https://doi.org/10.1093/jxb/ery285

Rankin, K.E., Hazell, Z.J., Middleton, A.M., Mavrogordato, M.N., 2021. Micro-focus X-ray CT scanning of two rare wooden objects from the wreck of the London, and its application in heritage science and conservation. J. Archaeol. Sci. Rep. 39, 103158. https://doi.org/10.1016/j.jasrep.2021.103158

Rathgeber, C.B.K., Cuny, H.E., Fonti, P., 2016. Biological Basis of Tree-Ring Formation: A Crash Course. Front. Plant Sci. 7. https://doi.org/10.3389/fpls.2016.00734

Richter, M., 2005. Three polychrome Japanese Buddhist sculptures from the Kamakura period: The scientific examination of layer structures, ground materials, pigments, metal leafs, and powders, in: Scientific Research on the Pictorial Arts of Asia–Proceedings of the Second Forbes Symposium at the Freer Gallery of Art. Archetype Publications Ltd London, pp. 21–34.

Salvemini, F., Grazzi, F., Kardjilov, N., Manke, I., Scherillo, A., Roselli, M.G., Zoppi, M., 2020. Non-invasive characterization of ancient Indonesian Kris through neutron methods. Eur. Phys. J. Plus 135, 1–25. https://doi.org/10.1140/epjp/s13360-020-00452-2

Schindelin, J., Arganda-Carreras, I., Frise, E., Kaynig, V., Longair, M., Pietzsch, T., Preibisch, S., Rueden, C., Saalfeld, S., Schmid, B., Tinevez, J.-Y., White, D.J., Hartenstein, V., Eliceiri, K., Tomancak, P., Cardona, A., 2012. Fiji: an

open-source platform for biological-image analysis. Nat. Methods 9, 676–682. https://doi.org/10.1038/nmeth.2019

Schlüter, S., Leuther, F., Vogler, S., Vogel, H.-J., 2016. X-ray microtomography analysis of soil structure deformation caused by centrifugation. Solid Earth 7, 129–140. https://doi.org/10.5194/se-7-129-2016

Shibui H., Sano Y., 2022. Observations of Bark Tissues of 12 Angiospermous Trees by Soft X-ray Photography. Mokuzai Gakkaishi 68, 107–116. (in Japanese). https://doi.org/10.2488/jwrs.68.107

Spicer, R., 2016. Variation in Angiosperm wood structure and its physiological and evolutionary significance, in: Groover, A., Cronk, Q. (Eds.), Comparative and Evolutionary Genomics of Angiosperm Trees, Plant Genetics and Genomics: Crops and Models. Springer International Publishing, Cham, pp. 19–60. https://doi.org/10.1007/7397_2016_28

Steppe, K., Cnudde, V., Girard, C., Lemeur, R., Cnudde, J.-P., Jacobs, P., 2004. Use of X-ray computed microtomography for non-invasive determination of wood anatomical characteristics. J. Struct. Biol. 148, 11–21. https://doi.org/10.1016/j.jsb.2004.05.001

Stock, S.R., 2008. Recent advances in X-ray microtomography applied to materials. Int. Mater. Rev. 53, 129–181. https://doi.org/10.1179/174328008X277803

Tan, J., Gao, Y., Liang, Z., Cao, W., Pomeroy, M.J., Huo, Y., Li, L., Barish, M.A., Abbasi, A.F., Pickhardt, P.J., 2020. 3D-GLCM CNN: A 3-dimensional gray-level co-occurrence matrix-based CNN model for polyp classification via CT colonography. IEEE Trans. Med. Imaging 39, 2013–2024. https://doi.org/10.1109/TMI.2019.2963177

Taylor, Z.J., Gurka, R., Kopp, G.A., Liberzon, A., 2010. Long-duration time-resolved PIV to study unsteady aerodynamics. IEEE Trans. Instrum. Meas. 59, 3262–3269. https://doi.org/10.1109/TIM.2010.2047149

Tazuru, S., Sugiyama, J., 2019. Wood identification of Japanese Shinto deity statues in Matsunoo-taisha Shrine in Kyoto by synchrotron X-ray microtomography and conventional microscopy methods. J. Wood Sci. 65, 60. https://doi.org/10.1186/s10086-019-1840-2

Thinley, C., Palmer, G., Vanclay, J.K., Thinley, C., Henson, M., 2005. Spiral and interlocking grain in *Eucalyptus dunnii*. Holz Als Roh- Werkst. 63, 372–379. https://doi.org/10.1007/s00107-005-0011-x

Thomas, J., Dijkstra, S.M., Harrington, J.J., Collings, D.A., 2022. Induction of compression wood inhibits development of spiral grain in radiata pine. IAWA J. (published online ahead of print 2022). https://doi.org/10.1163/22941932-bja10088

van der Walt, S., Schönberger, J.L., Nunez-Iglesias, J., Boulogne, F., Warner, J.D., Yager, N., Gouillart, E., Yu, T., 2014. scikit-image: image processing in Python. PeerJ 2, e453. https://doi.org/10.7717/peerj.453

van Duuren, D., 1998. The Kris: An Earthly Approach to a Cosmic Symbol. Pictures Publishers.

Vansteenkiste, D., Van Acker, J., Stevens, M., Le Thiec, D., Nepveu, G., 2007. Composition, distribution and supposed origin of mineral inclusions in

sessile oak wood — consequences for microdensitometrical analysis. Ann. For. Sci. 64, 11–19. https://doi.org/10.1051/forest:2006083
Wang, Q., Liu, X., Yang, S., Jiang, M., Cao, J., 2019. Non-destructive detection of density and moisture content of heartwood and sapwood based on X-ray computed tomography (X-CT) technology. Eur. J. Wood Wood Prod. 77, 1053–1062. https://doi.org/10.1007/s00107-019-01459-y
Wheeler, E.A., Baas, P., 1998. Wood Identification -A Review. IAWA J. 19, 241–264. https://doi.org/10.1163/22941932-90001528
Wijayatno, W., Sudrajat, U. (Eds.), 2011. Keris dalam perspektif Keilmuan [Kris in scientific perspective]. Direktorat Jendral Kebudayaan, Jakarta.
Withers, P.J., Bouman, C., Carmignato, S., Cnudde, V., Grimaldi, D., Hagen, C.K., Maire, E., Manley, M., Du Plessis, A., Stock, S.R., 2021. X-ray computed tomography. Nat. Rev. Methods Primer 1, 18. https://doi.org/10.1038/s43586-021-00015-4
Wong, A.D., Searson, P.C., 2014. Live-cell imaging of invasion and intravasation in an artificial microvessel platform. Cancer Res. 74, 4937–4945. https://doi.org/10.1158/0008-5472.CAN-14-1042
Worbes, M., 2011. Wood Anatomy and Tree-Ring Structure and Their Importance for Tropical Dendrochronology, in: Junk, W.J., Piedade, M.T.F., Wittmann, F., Schöngart, J., Parolin, P. (Eds.), Amazonian Floodplain Forests: Ecophysiology, Biodiversity and Sustainable Management. Springer Netherlands, Dordrecht, pp. 329–346. https://doi.org/10.1007/978-90-481-8725-6_17
Youming, X., Zehui, J., Benhua, F., Han, L., 2001. Variation of wood properties within and between camphor tree plantation and their predicting models. Sci. Silvae Sin. 37, 92–98.
Zheng, J., Martínez-Cabrera, H.I., 2013. Wood anatomical correlates with theoretical conductivity and wood density across China: evolutionary evidence of the functional differentiation of axial and radial parenchyma. Ann. Bot. 112, 927–935. https://doi.org/10.1093/aob/mct153

Acknowledgements

I would like to express deeply gratitude to my supervisor, Professor Junji Sugiyama (Laboratory of Tree Cell Biology), for his invaluable guidance, encouragement, motivation, and inspiration throughout my research.

I am deeply grateful to Professor Yoshihisa Fujii and Professor Masashi Nakamura for their invaluable contributions to my thesis, including their critical reading, valuable suggestions, and time spent examining it.

I would like to express my sincere appreciation to the Ministry of Education, Culture, Sport, Science, and Technology (MEXT) for providing me with the opportunity and financial support during my doctoral course at Kyoto University. Their support was essential in enabling me to complete my research.

I am deeply appreciative of the scientific guidance and support provided by Associate Professor Arata Yoshinaga and Assistant Professor Tatsuya Awano during my work at the Laboratory of Tree Cell Biology. I would also like to extend my appreciation to all the student members of the Laboratory of Tree Cell Biology for their friendship, advice, assistance, and engaging discussions throughout my time at the laboratory. I would also like to extend my gratitude to Ms. Misa Moriyasu for her consistent help, particularly with administrative tasks.

I would like to express my appreciation Professor Tomoya Imai, Junior Associate Professor Suyako Tazuru, Assistant Professor Kei'ichi Baba for their support during my time at Laboratory of Biomass Morphogenesis and Information (now known as Laboratory of Material Biology). I also thank to Ms. Nanako Sugano. Her assistance with administrative tasks was particularly invaluable. I would also like to express my gratitude to Ms. Izumi Kanai and Mr. Hajime Sorimachi for their invaluable technical assistance during my research

I would like to express my sincere gratitude to Dr. Tomoyuki Fujii from FFPRI, as well as Dr. Ratih Damayanti and Dr. Listya M. Dewi from FORDA, for the materials and insight he provided for a portion of my study. I would also like to thank Mr. Tominori Araki and Mr. Masahiro Miyata from Tokyo National Museum, as well as Prof. Imazu Setsuo and Dr. Torigoe Toshiyuki from Kyushu National Museum for their assistance in providing the facility and help for a portion of the experiment.

I am deeply appreciative of the guidance and support provided by Dr. Kayoko Kobayashi, Dr. Soon-Wook Hwang, Dr. Shuoye Chen and Dr. Shingo Kiyoto in overcoming my research challenges.

I am also deeply grateful to my friends and colleagues for their support during my time in Kyoto. I would also like to extend my sincerest thanks to PPI Kyoto-Shiga for their support since my first-time arrival in Japan in 2016. I am deeply grateful to Ms. Raufelina Febriama for her invaluable help, support, and motivation in helping me to complete this study.

I am deeply grateful to Dr. Widyanto Dwi Nugroho for his invaluable guidance during my pursuit of my master's and doctoral degrees. I would also like to thank Dr. Fajar Waskito and Mr. Taufiq Hermawan for providing the samples that were used in my research. Their generosity and assistance were greatly appreciated.

I would like to thank my family for their unwavering support and dedicate this work to my late younger brother, Heiri Hidayat, that passed away in 2021.

Finally, I would like to acknowledge that this work would not have been possible without the support and help of all the individuals who have contributed to it. I apologize that I cannot mention everyone by name, but please know that I am deeply grateful for all of your contributions. From the bottom of my heart, I thank you all for your support and guidance throughout my research.

List of Publications

1. Hairi Cipta, Widyanto Dwi Nugroho, Suyako Tazuru, Junji Sugiyama. Identification of the wood species in the wooden sheath of Indonesian kris by synchrotron X-ray microtomography. Journal of Wood Science, Volume 68, Article number: 65.
   DOI: https://doi.org/10.1186/s10086-022-02072-z
   Corresponding Chapter: Chapter 2

2. Hairi Cipta, Kayoko Kobayashi, Shuoye Chen, Junji Sugiyama (2022) Examination of *Cinnamomum camphora* interlocked grain adopting X-ray computed tomography combined with particle image velocimetry. Journal of Wood Science, Volume 68, Article number: 56.
   DOI: https://doi.org/10.1186/s10086-022-02064-z
   Corresponding Chapter: Chapter 4